

Numerical Investigation of Observational Flux Partitioning Methods for Water Vapor and Carbon Dioxide

Einara Zahn¹, Khaled Ghannam^{2,3}, Marcelo Chamecki⁴, Arnold F. Moene⁵, William P. Kustas⁶, Stephen Good⁷, Elie Bou-Zeid¹

¹Department of Civil and Environmental Engineering, Princeton University, Princeton, New Jersey, USA
²Program in Atmospheric and Oceanic Sciences (Cooperative Institute for Modeling the Earth System),

Princeton University, Princeton NJ, USA

³Department of Civil and Environmental Engineering, Northeastern University, Boston, MA

⁴Department of Atmospheric & Oceanic Sciences, University of California in Los Angeles, Los Angeles,

California, USA

⁵Meteorology and Air Quality Group, Wageningen University and Research, Wageningen, The

Netherlands

⁶USDA-ARS, Hydrology and Remote Sensing Lab, Beltsville, MD 20705-2350, USA

⁷Department of Biological and Ecological Engineering, Oregon State University, Corvallis, OR 97331,

USA

Key Points:

- The performance of four partitioning methods are explored with aid of large-eddy simulations
- The methods' performance are shown to depend on flux ratios, canopy sparseness, and measurement height
- The correlation coefficient between CO₂ and water vapor is shown to help inform the choice of water-use efficiency models

24 **Abstract**

25 While yearly budgets of CO_2 flux (F_c) and evapotranspiration (ET) above vegetation
 26 can be readily obtained from eddy-covariance measurements, the separate quantification
 27 of their soil (respiration and evaporation) and canopy (photosynthesis and transpiration)
 28 components remains an elusive yet critical research objective. In this work, we investi-
 29 gate four methods to partition observed total fluxes into soil and plant sources: two new
 30 and two existing approaches that are based solely on analysis of conventional high fre-
 31 quency eddy-covariance (EC) data. The physical validity of the assumptions of all four
 32 methods, as well as their performance under different scenarios, are tested with the aid
 33 of large-eddy simulations, which are used to replicate eddy-covariance field experiments.
 34 Our results indicate that canopies with large, exposed soil patches increase the mixing
 35 and correlation of scalars; this negatively impacts the performance of the partitioning
 36 methods, all of which require some degree of uncorrelatedness between CO_2 and water
 37 vapor. In addition, best performances for all partitioning methods were found when all
 38 four flux components are non-negligible, and measurements are collected close to the canopy
 39 top. Methods relying on the water-use efficiency (W) perform better when W is known
 40 a priori, but are shown to be very sensitive to uncertainties in this input variable espe-
 41 cially when canopy fluxes dominate. We conclude by showing how the correlation co-
 42 efficient between CO_2 and water vapor can be used to infer the reliability of different W
 43 parameterizations.

44 **Plain Language Summary**

45 Forests and vegetated ecosystems play a crucial role in the water and carbon cy-
 46 cles. During the day, plants absorb CO_2 through photosynthesis (P), releasing water va-
 47 por via transpiration (T). On the other hand, the soil underneath contributes to CO_2
 48 through respiration (R), and moist soil leads to water evaporation (E). While meteo-
 49 rological towers currently measure total CO_2 ($F_c = P + R$) and water vapor ($ET =$
 50 $E + T$) exchanges, distinguishing the contributions from soil respiration and evapora-
 51 tion versus tree photosynthesis and transpiration remains a challenge. This study ad-
 52 dresses this gap by investigating methods to separate F_c and ET into their individual
 53 components. Using a simulated forest environment with a virtual meteorological tower,
 54 the study tests four methods to estimate respiration, photosynthesis, evaporation, and
 55 transpiration. Results reveal that more reliable estimates are obtained when measure-
 56 ments are collected close to the forest top, especially in the absence of significant veg-
 57 etation gaps that lead to strong mixing. Additionally, the study highlights the expected
 58 errors in two approaches when faced with real-world uncertainties. By elucidating op-
 59 timal conditions for method application, this research contributes to advancing our un-
 60 derstanding of ecosystem-atmosphere interactions and informs the accurate measurement
 61 of vital components in the carbon and water cycles.

62 **1 Introduction**

63 Land-atmosphere exchanges of water vapor and CO_2 are important components
 64 of the global water and carbon cycles. In this context, vegetated canopies play an im-
 65 portant role in both cycles through their contributions to evapotranspiration (ET) and
 66 net CO_2 exchange (F_c). Facilitated by an extensive network of eddy-covariance (EC) tow-
 67 ers setup across the globe, we are currently able to quantify the long-term budgets for
 68 both quantities over many land use types (Balocchi et al., 2001; Balocchi, 2003; Hollinger
 69 et al., 2004; Fisher et al., 2008; Novick et al., 2018; Balocchi et al., 2024). Nonetheless,
 70 long-term quantification of their individual soil (evaporation and respiration) and plant
 71 canopy (transpiration and photosynthesis) components is an equally important but much
 72 more challenging research goal. While different methods have been proposed to measure
 73 one or more of these components (Law et al., 1999; Wilson et al., 2001; Roupsard et al.,

2006; Paul-Limoges et al., 2017; Stoy et al., 2019; Paul-Limoges et al., 2020), such as soil chambers, sap-flow, leaf-level measurements, and concurrent bellow and above canopy eddy-covariance measurements, they are still unable to offer unified long-term measurements (yearly scale) of all components across different ecosystems. This poses a challenge to understanding, for instance, how different environmental, meteorological, and climatological conditions affect these processes, which are urgent research questions as we attempt to mitigate and adapt to climate change and variability (Mengis et al., 2015; Kirschbaum & McMillan, 2018; Dusenge et al., 2019; Baslam et al., 2020; Wang et al., 2022). Therefore, the development and implementation of practical and accurate methods to partition the observed total ET and F_c fluxes remains a significant objective, particularly if such methods can rely solely on eddy-covariance data and can thus be widely applicable to ongoing measurements.

For partitioning CO_2 components, several methods have been proposed; some, for example, rely on modeling soil respiration (R_{soil}) and computing the plant component as the residual $F_c - R_{soil} = GPP$, which is referred to as the gross primary productivity (Reichstein et al., 2005; Lasslop et al., 2010). Various approaches (physical and machine learning based) have also emerged to partition total measured ET into plant transpiration (T) and soil evaporation (E) (Zhou et al., 2016; Wei et al., 2017; Scott & Biederman, 2017; Perez-Priego et al., 2018; Nelson et al., 2018; Rigden et al., 2018; X. Li et al., 2019; Eichelmann et al., 2022). However, challenges in model validation have prevented a clear assessment of their accuracy, as illustrated by divergent partitioning estimates in comparison studies (Nelson et al., 2020). Furthermore, these ET partitioning methods often require additional uncertain parameterizations and/or depend on hard-to-measure, and often unavailable, environmental variables. Specifically, many require *a priori* knowledge of the GPP , itself an unknown that requires F_c partitioning models as discussed above. Consequently, approaches capable of simultaneously partitioning F_c and ET offer distinct advantages over existing methods that tackle these fluxes separately, given their intrinsic physical connections.

A particularly useful class of partitioning methods, that this paper focuses on, are approaches based on turbulent statistics computed from high-frequency data. Not only do they require few (usually only water-use efficiency) or no extra inputs, but they also allow the simultaneous and consistent partitioning of ET and F_c flux components. Three previously proposed methods are the flux-variance similarity (FVS) (Scanlon & Sahu, 2008; Scanlon & Kustas, 2010; Scanlon et al., 2019), the modified relaxed-eddy accumulation (MREA) (Thomas et al., 2008; Zahn et al., 2022), and the conditional eddy covariance (CEC) (Zahn et al., 2022). Cognizant of potential limitations of FVS, CEC, and MREA, in the present study we also formulate and test two new but related approaches. The first approach is the conditional eddy accumulation or CEA, which combines quadrant analyses and the traditional Relaxed Eddy Accumulation method (Businger & Oncley, 1990). While it uses similar principles as adopted by MREA and CEC, CEA's formulation also includes downdrafts in its framework, and yields different results. The second method is a hybrid approach that assimilates W into the CEC method, and is here called CECw. The idea behind CECw is to investigate how much skill the water-use efficiency alone adds to partitioning.

Previous work comparing two or more of these EC-based methods (Klosterhalfen, Graf, et al., 2019; Klosterhalfen, Moene, et al., 2019; Zahn et al., 2022) across sites have highlighted their potential. Nonetheless, a general conclusion regarding their applicability across different ecosystems was not attained, in part because of the challenge in validating these methods' formulations and results. In addition, assessing their limitations — *i.e.*, when and where they do not perform well — would require tower data across a wide range of ecosystem types and climatic conditions that could result in various combinations of flux component strengths. To overcome limitations of field experiments in answering many of the open research questions, in this study we use numerical simula-

127 tions of canopy flows relying on the Large-Eddy Simulations (LES) (Stoll et al., 2020)
 128 technique. One of the biggest advantages LES offers in the present study is that the true
 129 flux components and water-use efficiency are known inputs; therefore, the results and
 130 underlying assumptions for the implemented partitioning methods, which are applied to
 131 time series sampled during the simulation, can be validated.

132 Equipped with numerical simulations over a wide range of flow conditions, we are
 133 now able to answer more specific questions that experimental data alone cannot. One
 134 important open subject of inquiry with these multiple available approaches is under what
 135 conditions (measurement height, season, canopy characteristics, etc.) are some approaches
 136 more accurate than others. As discussed by Zahn et al. (2022), the assumption that ed-
 137 dies with a signal from the soil can be distinguished from those originating from the plant
 138 canopy would suggest that more realistic results should be obtained for both methods
 139 over sparser canopies (a conclusion we will revisit here). The authors also concluded that
 140 the high-frequency data should be measured as close as possible to the canopy so as to
 141 sample the transporting eddies before turbulence mixes canopy and soil fluxes. However,
 142 it remains unclear whether sparser canopies would allow a higher measurement point given
 143 the stronger horizontal segregation between canopy and soil. The importance of plant
 144 canopy “openness” is thus investigated in the present simulations. Another related knowl-
 145 edge gap is how (not if) the methods’ performances are affected by the relative magni-
 146 tude of soil versus canopy fluxes. To address this, we investigate a broad range of com-
 147 binations of the ratios of photosynthesis/respiration and transpiration/evaporation, and
 148 how they influence the outcome of each method.

149 Overall, this paper explores how similarity-based partitioning approaches perform
 150 under various conditions encountered in real field experiments, and how simple turbu-
 151 lence measurements can help elucidate the biophysiological behavior of plant canopies.
 152 The specific following questions frame our investigation

- 153 1. How does the sparseness of the canopy impact the assumptions of the methods
 154 and their performance?
- 155 2. How does the magnitude of the individual four flux components influence parti-
 156 tioning skill?
- 157 3. What is the role of the measurement height for different levels of canopy sparse-
 158 ness?
- 159 4. How sensitive are the FVS and CECw methods to errors in water-use efficiency?

160 The answers to these questions will further deepen our understanding of ET and F_c par-
 161 titioning and the reliability of the investigated methods. They will also help to broadly
 162 identify the best practices for future experimental campaigns aimed at obtaining flux com-
 163 ponent estimates.

164 2 Theory

165 We start this section with a brief summary of the partitioning methods investigated,
 166 where the main equations and necessary inputs are discussed. Throughout the text, the
 167 concentrations of CO_2 and H_2O are defined as c and q , respectively. The velocity com-
 168 ponents in the streamwise (x), cross-stream (y), and vertical directions (z) are u , v , and
 169 w , while the deviation of a variable μ around its time and/or space average $\bar{\mu}$ is denoted
 170 using a prime $\mu' = \mu - \bar{\mu}$. An important note is that, for the remainder of the paper,
 171 we will not distinguish between soil and plant respiration. All the tested methods can-
 172 not make this distinction either since they are interrogating the properties of air parcels
 173 coming from the plants with the lumped information about gross primary production
 174 (GPP , which is the net carbon uptake by the plants accounting for their potential res-
 175piration), and thus they partition net ecosystem exchange into GPP and soil respi-
 176 ration, R_{soil} . In our LES setup and the rest of the paper, however, CO_2 will be emitted

177 from the soil only, and we will refer to it as R , while the simulated plants only assimilate CO₂, and we refer to that flux as photosynthesis (P).
178

179 2.1 Brief description of the partitioning methods

180 In what follows, a summary of the FVS, CEC, and the newly proposed CEA and
181 CECw, is presented. We note that results for the MREA method, previously explored
182 in Zahn et al. (2022), were almost identical to CEC and thus will not be reported in this
183 paper.

184 2.1.1 Flux-variance similarity (FVS) method

185 The flux-variance similarity method combines the similarity equations for variances
186 of c and q with the water-use efficiency $W = P/T$ (Scanlon & Sahu, 2008; Scanlon &
187 Kustas, 2010). More specifically, it rewrites the budgets by separating the two scalars
188 into their soil (c_r for respiration and q_e for evaporation) and canopy (c_p for photosyn-
189 thesis and q_t for transpiration) components. To close the system of equations, the fol-
190 lowing approximations are needed (Katul et al., 1995)

$$191 \rho_{c_p, c_r} \approx \frac{\rho_{w, c_r}}{\rho_{w, c_p}} \quad \text{and} \quad \rho_{q_t, q_e} \approx \frac{\rho_{w, q_e}}{\rho_{w, q_t}}, \quad (1)$$

192 where $\rho_{a,b}$ is the correlation coefficient between the variables a and b . After some alge-
193 bra, the final equations for the ratios of flux components are

$$194 \frac{E_{\text{FVS}}}{T_{\text{FVS}}} = -\rho_{c_p, c_r}^2 + \rho_{c_p, c_r}^2 \sqrt{1 - \rho_{c_p, c_r}^{-2} \left(1 - W^2 \sigma_q^2 / \sigma_{c_p}^2\right)}, \quad (2a)$$

$$195 \frac{R_{\text{FVS}}}{P_{\text{FVS}}} = -\rho_{c_p, c_r}^2 \pm \rho_{c_p, c_r}^2 \sqrt{1 - \rho_{c_p, c_r}^{-2} \left(1 - \sigma_c^2 / \sigma_{c_p}^2\right)}, \quad (2b)$$

196 where ρ_{c_p, c_r} and σ_{c_p} , the standard deviation of c_p , are directly computed by the two fol-
197 lowing complementary equations (Skaggs et al., 2018; Scanlon et al., 2019),

$$198 \sigma_{c_p}^2 = \frac{(1 - \rho_{c,q}^2) (\sigma_q \sigma_c W)^2 \left(\sigma_q^2 \overline{w'c'}^2 - 2\rho_{c,q} \sigma_q \sigma_c \overline{w'c'} \overline{w'q'} + \sigma_c^2 \overline{w'q'}^2\right)}{\left[\sigma_c^2 \overline{w'q'} + \sigma_q^2 \overline{w'c'} W - \rho_{c,q} \sigma_q \sigma_c (\overline{w'c'} + \overline{w'q'} W)\right]^2}, \quad (3)$$

$$199 \rho_{c_p, c_r}^2 = \frac{(1 - \rho_{c,q}^2) \sigma_q^2 \sigma_c^2 \left(\overline{w'c'} - \overline{w'q'} W\right)^2}{\left(\sigma_q^2 \overline{w'c'}^2 - 2\rho_{c,q} \sigma_q \sigma_c \overline{w'q'} \overline{w'c'} + \sigma_c^2 \overline{w'q'}^2\right) (\sigma_c^2 - 2\rho_{c,q} \sigma_q \sigma_c W + \sigma_q^2 W^2)}. \quad (4)$$

200 The standard deviation of c , σ_c , and q , σ_q , and the correlation coefficient between c and
201 q , $\rho_{c,q}$, are also needed and can be directly computed from the measured time series. The
202 water-use efficiency — which is an input to the method — must be separately measured
203 or estimated (a description of how to parameterize W can be found elsewhere (Scanlon
204 & Kustas, 2010; Skaggs et al., 2018; Zahn et al., 2022)). For our numerical simulations,
205 W is a known input. However, even the correct water-use efficiency will only result in
206 realistic solutions if the following conditions are met (Scanlon et al., 2019)

$$207 \rho_{c,q}^{-1} \frac{\sigma_c}{\sigma_q} \leq \frac{\overline{w'c'}}{\overline{w'q'}} < \rho_{c,q} \frac{\sigma_c}{\sigma_q} \quad \text{for } \rho_{c,q} < 0, \text{ and} \quad (5a)$$

$$208 \frac{\overline{w'c'}}{\overline{w'q'}} < \rho_{c,q} \frac{\sigma_c}{\sigma_q} \quad \text{for } \rho_{c,q} > 0. \quad (5b)$$

209 Failure to meet the conditions outlined above has been identified as the primary rea-
210 son for the limited availability of physically valid solutions across various sites, with stud-
211 ies (Sulman et al., 2016; Klosterhalfen, Graf, et al., 2019; Wagle et al., 2021; Zahn et al.,
212 2022) reporting success rates as low as 30%.

213 **2.1.2 Conditional eddy covariance (CEC) method**

214 The conditional eddy covariance method (Zahn et al., 2022) builds on the MREA
 215 framework proposed by Thomas et al. (2008). Similarly to MREA, CEC conditionally
 216 samples ejections originating from the soil that are rich in CO₂ and H₂O ($w' > 0$, $c' >$
 217 0, and $q' > 0$); in addition, it also samples ejections that were in contact with the canopy
 218 and are depleted in CO₂ but enriched in water vapor ($w' > 0$, $c' < 0$, and $q' > 0$),
 219 which is not done in the MREA framework. The data points of a time series of length
 220 N that are identified to be in contact with soil or canopy are then used to compute “sam-
 221 ple” fluxes of evaporation (f_E) and respiration (f_R) or transpiration (f_T) and photosyn-
 222 thesis (f_P) (see Figure 1 in Zahn et al. (2022)). These sample fluxes are given by the fol-
 223 lowing expressions

$$224 \quad f_E = \frac{1}{N} \sum I_S w' q' \quad \text{and} \quad f_R = \frac{1}{N} \sum I_S w' c' \quad (6)$$

$$225 \quad f_T = \frac{1}{N} \sum I_C w' q' \quad \text{and} \quad f_P = \frac{1}{N} \sum I_C w' c', \quad (7)$$

226 where I_S is an indicator function that selects only “soil surface eddies”, *i.e.*, instanta-
 227 neous data points that satisfy $c' > 0, q' > 0, w' > 0$; I_C , on the other hand, selects
 228 only eddies that were in touch with the canopy where we expect $c' < 0, q' > 0, w' >$
 229 0. Sample fluxes were only computed when the respective quadrant contained at least
 230 2% of the total data points for the averaging period. If, on the other hand, $\sum I_S/N <$
 231 2% (or $\sum I_C/N < 2\%$), we attribute all fluxes to canopy (or soil) components.

232 The expressions given in (6) and (7) are not the actual fluxes of each component;
 233 instead, they are assumed to be “sample” indicative fluxes that we can use to estimate
 234 the ratio of the total fluxes by the following:

$$235 \quad r_{ET} = \frac{f_E}{f_T} = \frac{E_{CEC}}{T_{CEC}} \quad \text{and} \quad r_{RP} = \frac{f_R}{f_P} = \frac{R_{CEC}}{P_{CEC}}. \quad (8)$$

236 The separate flux components are then obtained by combining the flux ratios with the
 237 expressions for total fluxes ($ET = T + E$ and $F_c = R + P$). However, as discussed by
 238 Zahn et al. (2022), a mathematical constraint (division by zero) happens whenever $\frac{R_{CEC}}{P_{CEC}} \approx$
 239 -1 , but affects only the partitioning for CO₂ flux components. Because the FVS method
 240 also computes the flux ratios, the same mathematical constraint arises when $\frac{R_{FVS}}{P_{FVS}} \approx$
 241 -1 . Therefore, solutions in this limit must be carefully inspected (and removed) for both
 242 methods.

243 **2.1.3 Conditional Eddy Accumulation (CEA) method**

244 The traditional Relaxed Eddy Accumulation method (Businger & Oncley, 1990)
 245 was derived as an alternative to eddy-covariance measurements for scalars s that can-
 246 not be measured at a high frequency. The method consists of separately measuring the
 247 average scalar concentrations associated with updrafts (\bar{s}^+) and concentrations associ-
 248 ated with downdrafts (\bar{s}^-), estimating the total scalar flux (F_s) as

$$249 \quad F_s = \beta \sigma_w (\bar{s}^+ - \bar{s}^-), \quad (9)$$

250 where σ_w is the standard deviation of the vertical velocity and β is a constant.

251 By taking into account only updrafts rich in CO₂ and H₂O, Thomas et al. (2008)
 252 modified equation (9) and proposed the MREA method. The CEA method, on the other
 253 hand, retains the information from downdrafts and estimates an analogue to \bar{s}^+ and \bar{s}^-
 254 for each individual flux component. In the framework proposed here, we compute \bar{c}_r^+ and
 255 \bar{q}_e^+ (using $c' > 0, q' > 0, w' > 0$) and \bar{c}_r^- and \bar{q}_e^- ($c' < 0, q' < 0, w' < 0$), both repre-
 256 senting respiration and evaporation (note that the fluxes in both cases are positive). For
 257 canopy components, we compute \bar{c}_p^+ and \bar{q}_p^+ ($c' < 0, q' > 0, w' > 0$) and \bar{c}_p^- and

258 and $\overline{q_t^-}$ ($c' > 0, q' < 0, w' < 0$), where the fluxes are now negative for c (photosynthesis) and positive for q (transpiration). These conditional averages are computed as
259

$$260 \quad \overline{c_r^+} = \frac{1}{N_S^+} \sum c' I_S^+ \quad \text{and} \quad \overline{q_e^+} = \frac{1}{N_S^+} \sum q' I_S^+, \quad (10)$$

$$261 \quad \overline{c_r^-} = \frac{1}{N_S^-} \sum c' I_S^- \quad \text{and} \quad \overline{q_e^-} = \frac{1}{N_S^-} \sum q' I_S^-, \quad (11)$$

$$262 \quad \overline{c_p^+} = \frac{1}{N_C^+} \sum c' I_C^+ \quad \text{and} \quad \overline{q_t^+} = \frac{1}{N_C^+} \sum q' I_C^+, \quad (12)$$

$$263 \quad \overline{c_p^-} = \frac{1}{N_C^-} \sum c' I_C^- \quad \text{and} \quad \overline{q_t^-} = \frac{1}{N_C^-} \sum q' I_C^-, \quad (13)$$

264 where N and I are the number of sampled events and the indicator functions defined according
265 to the origin of fluxes (subscript ‘S’ for soil and ‘C’ for canopy), as defined for
266 the CEC method but not also separated by updrafts (+) and downdrafts (-).

267 By assuming that the coefficient β is constant or weakly dependent on stability (Businger
268 & Oncley, 1990; Katul et al., 1996; Zahn et al., 2023; Allouche et al., 2023), and that σ_w
269 is the same regardless of conditional sampling, we approximate the flux ratios as

$$270 \quad r_{ET} = \frac{E_{CEA}}{T_{CEA}} = \frac{\overline{q_e^+} - \overline{q_e^-}}{\overline{q_t^+} - \overline{q_t^-}}, \quad (14)$$

$$271 \quad r_{RP} = \frac{R_{CEA}}{P_{CEA}} = \frac{\overline{c_r^+} - \overline{c_r^-}}{\overline{c_p^+} - \overline{c_p^-}}. \quad (15)$$

272 A diagram illustrating the method is shown in Figure 1, where we plot points classified
273 following the conditional sampling, as well as the average values as defined in (10)–
274 (13). When plant components dominate the fluxes (E and R), we expect the denominator
275 in (14) and (15) to be larger, as indicated in plot 1a and b; however, for fluxes dominated
276 by soil components, the numerators are larger (plot 1c and 1d).

277 2.1.4 Combining CEC and water-use efficiency

278 Both CEC and CEA have the practical advantage of not requiring *a priori* knowledge of the water-use efficiency. However, if W is known, it can in fact inform both methods. Therefore, we now combine the flux ratios as defined by the CEC method with the water-use efficiency and derive an alternative partitioning method that we will refer to as CECw. The goal of this new model is to investigate if, given the correct water-use efficiency, a simpler method could perform similarly to the FVS method, potentially being easier to implement and yielding solutions more often. Comparing CEC and CECw will then indicate how important the knowledge of W is to the skill of partitioning models in general, including for FVS.

287 We start the derivation by combining the water-use efficiency ($W = P/T$) and
288 the flux ratios as defined by CEC ($r_{RP} = R/P$ and $r_{ET} = E/T$),

$$289 \quad W = \frac{P}{T} = \frac{R}{E} \frac{r_{ET}}{r_{RP}} = Z \frac{r_{ET}}{r_{RP}}, \quad (16)$$

290 where we define $Z = R/E$.

291 Rewriting the equations for total fluxes and introducing the definitions of W and
292 Z , we have

$$293 \quad F_c = W \times T + R, \quad (17)$$

$$294 \quad T = ET - \frac{R}{Z}. \quad (18)$$

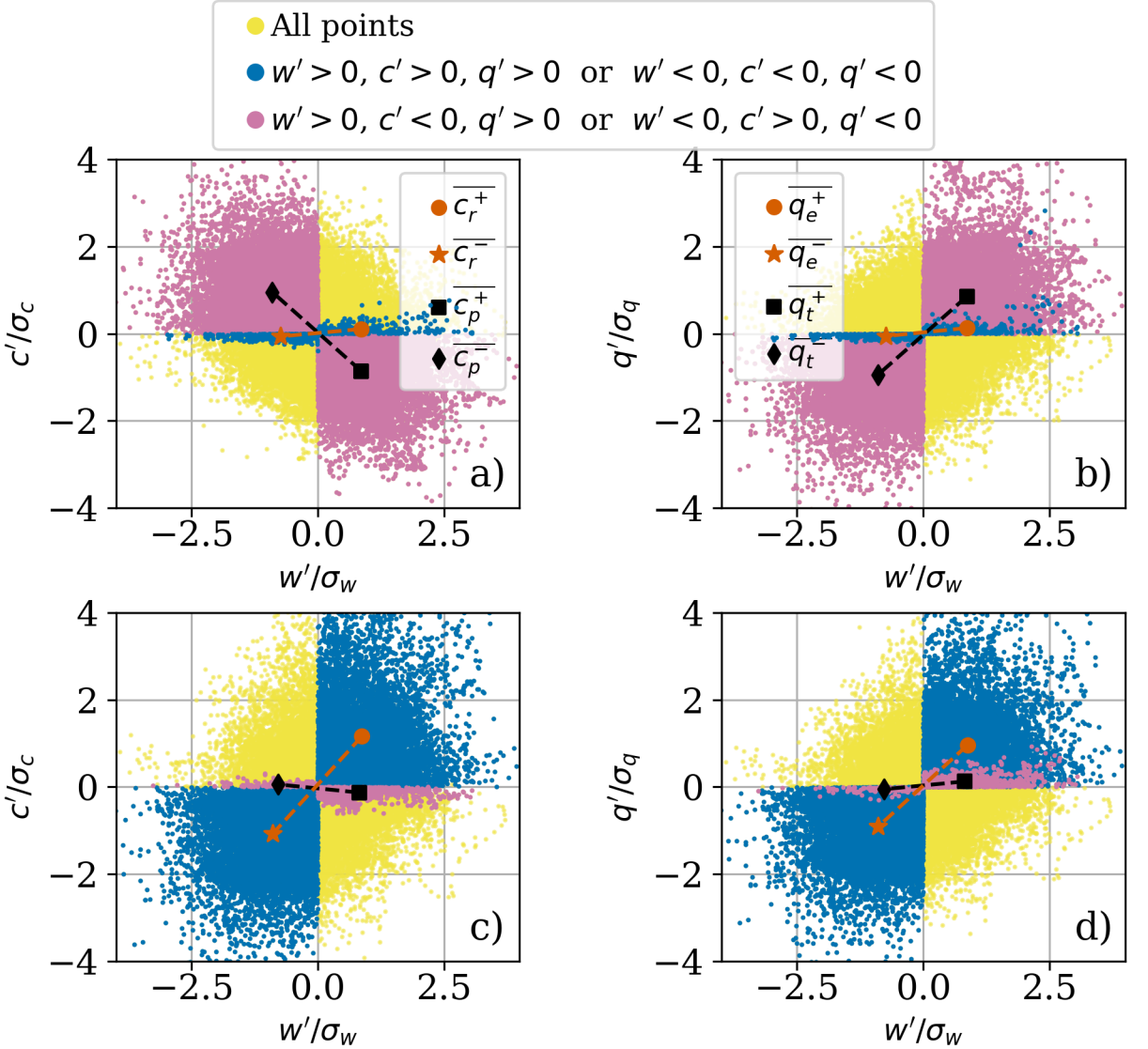


Figure 1. Quadrant plots illustrating the Conditional Eddy Accumulation (CEA) method, where the points selected to compute ratios in Eqs. (14) (plots a and c) and (15) (plots b and d) are shown. Figure generated using time series from large-eddy simulations. Plots a) and b) have ratios $T/E=|P|/R=5$, while plots c) and d) have ratios $T/E=|P|/R=0.2$.

295 Combining equations (17) and (18) and rewriting for R , we get the following expression
 296 for soil respiration

$$297 R_{CECw} = \frac{F_c - W \times ET}{1 - \frac{W}{Z}} = \frac{F_c - W \times ET}{1 - \frac{r_{ET}}{r_{RP}}}, \quad (19)$$

298 where the ratios r_{RP} and r_{ET} are computed from equations (6)–(8). Similarly, we can
 299 obtain an expression for T_{CECw}

$$300 T_{CECw} = \frac{F_c - W \times ET \times \frac{r_{RP}}{r_{ET}}}{1 - \frac{r_{RP}}{r_{ET}}}. \quad (20)$$

301 Corresponding expressions can be derived for P_{CECw} and E_{CECw} , or they can then be
 302 computed as the residuals of the total eddy-covariance (EC) fluxes (both approaches yield
 303 identical results since the total flux expression are directly used in the derivation). Be-
 304 cause $r_{ET} > 0$ and $r_{RP} < 0$, this equation has no mathematical singularity. Nonethe-
 305 less, under certain conditions the method can result in negative transpiration or respi-
 306 ration. Therefore, we must also ensure that $T_{CECw} > 0$ and $R_{CECw} > 0$. In addition,
 307 we also tested the method by computing the ratios following the CEA method (expres-
 308 sions (14) and (15)), deriving a CEAw method, but the results were similar to CECw
 309 and thus not included here.

310 3 Methods

311 This section describes the setup of our numerical simulations and how the time se-
 312 ries were sampled and processed for partitioning.

313 3.1 Numerical simulations of plant and soil contributions of CO₂ and 314 H₂O

315 Simulation of turbulence transport and time series sampling by virtual towers were
 316 conducted using large-eddy simulations (LES). To avoid the computational expenses of
 317 simulating the entire Atmospheric Boundary Layer (ABL, on the order of 1 km), we fol-
 318 lowed the guidelines of Zahn and Bou-Zeid (2023) to simulate only the Surface Layer (SL
 319 $\approx 10\%$ ABL) and ensure a high-resolution representation of the canopy. In addition, ev-
 320 ery simulation utilizes an identical sink/source flux profile and homogeneous and steady
 321 soil fluxes, which are only rescaled, as described below, to represent different combina-
 322 tions of flux components. The detailed description of our LES setup can be found in Ap-
 323 pendix A.

324 One of the main goals of our simulations is to reproduce (and sample) c and q un-
 325 der different combinations of canopy and soil fluxes. To decrease the number of simu-
 326 lations required to accomplish this task, we follow the approach adopted by Klosterhalfen,
 327 Moene, et al. (2019). First, we obtain four solutions for canopy (c_p and q_t) and soil (c_r
 328 and q_e) components separately, where $c = c_p + c_r$ and $q = q_e + q_t$. In these simula-
 329 tions, we ensure that plant components have a source or sink term representing canopy
 330 transpiration and photosynthesis, while their bottom wall boundary condition is set to
 331 zero flux for q_t and c_p . Soil components, on the other hand, have an imposed flux only
 332 at the bottom surface representing q_e and c_r .

333 Finally, and because the advection-diffusion equations we solve for these four scalar
 334 are linear, from a single simulation we can easily adjust the respective contributions of
 335 soil and plant components by simply multiplying the original statistics of c_p , c_r , q_t , and
 336 q_e by the respective scaling factors. Note that this is only possible if q is treated as a pas-
 337 sive scalar (otherwise the buoyant feedback from q on the velocity field will render the
 338 advective term in the scalar equation non-linear in q). Thus, all our simulations are neu-
 339 tral with respect to q . To further decrease the complexity of our simulations and inter-
 340 pretation of results, we also considered the flow neutral with respect to temperature, thus

341 simulating a fully neutral canopy flow (we discuss the potential influence of buoyancy
 342 in the conclusions.)

343 3.2 Domain configuration and data sampling

344 A summary of the main details of our simulations is shown in table 1. The domain
 345 contains $(N_x \times N_y \times N_z) = (384 \times 256 \times 128)$ grid points, and aspect ratios $(L_x/L_z,$
 346 $L_y/L_z) = (3,2)$, where L_z is vertical domain height. This setup results in $dx = dy =$
 347 dz . In addition, the ratio of the domain height to the canopy height, h , is $L_z/h = 8$,
 348 which is in the range ($L_z/h = 3-14$) commonly adopted in the literature for canopy flows
 349 (Shaw & Schumann, 1992; Su et al., 1998; Watanabe, 2004; Yue et al., 2007; Dupont &
 350 Brunet, 2008; Mao et al., 2008; Pan, Chamecki, & Isard, 2014; Chen et al., 2020). To
 351 ensure good resolution for the turbulence inside the canopy flow, we represent the canopy
 352 with $N_h = 16$ vertical grid points. Sensitivity test implementing different domain heights,
 353 aspect ratios, grid resolution, mean flow forcing, and soil roughness length z_0 all indicated
 354 that the partitioning results are not sensitive to these simulation design options.

Table 1. Parameters of our simulations. L_z , L_y , and L_x (m) are the dimensions in z , y , and x
 directions; N_z , N_y , and N_x are the number of grid points in the three directions, while N_h is the
 number of vertical grid points representing the canopy; dx , dy , and dz (m) are the grid spacing; h
 (m) is the canopy height; z_0 (m) is the roughness length of the soil surface; LAI is the leaf-area
 index; dt is the time step (s).

Simulation parameter	Units	Value
N_x, N_y, N_z	grid points	384, 256, 128
N_h	grid points	16
L_z	m	140
$L_x/L_z, L_y/L_z$		3, 2
dx, dy, dz	m	1.1
L_z/h		8
z_0/h		0.00285
LAI	$\text{m}^2 \text{m}^{-2}$	2.0
dt	s	0.01

355 The analyses shown in this study used both spatial and temporal statistics. The
 356 spatial statistics (averaged in the cross-stream direction and time) were sampled after
 357 the total kinetic energy in the domain and the flux profiles reached equilibrium. For the
 358 temporal statistics, we also included 24 virtual “eddy-covariance towers” across the do-
 359 main, where the velocity and all simulated scalars were sampled at all vertical grid points
 360 every 25 time steps (i.e., every 0.25 s). This is sufficient here since the smallest resolved
 361 eddy is $\sim 2dx = 2.2$ m and its advective time across a grid node at a mean wind speed
 362 of 1 m/s (see velocity profiles in B1) is thus 2.2 s; we thus sample the smallest eddies
 363 with about 9 measurements in time. To ensure convergence of the time series, we sam-
 364 pled over a period of approximately 20 domain-scale eddy turnover times (L_z/u_*).

365 To represent the canopy, we used the leaf-area density and the source profiles S_q
 366 (Figure 2) for water-vapor mixing ratio following Shaw and Schumann (1992) and Su et
 367 al. (1998). As in these studies, we also set the leaf-area index (LAI) to 2. The same source

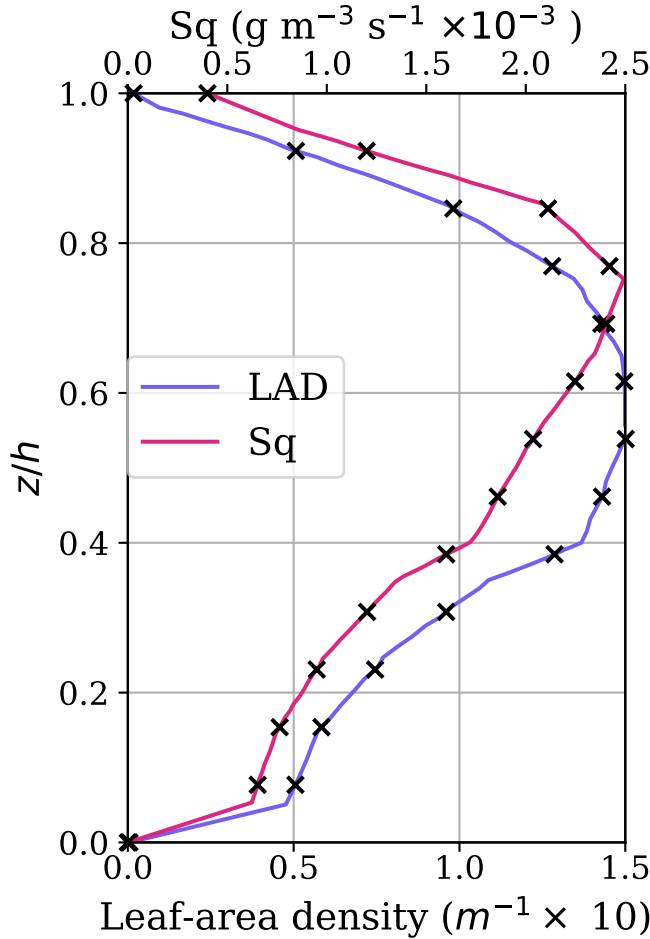


Figure 2. Leaf-area density (LAD) and source profile for water vapor mixing ratio imposed in the LES (Shaw & Schumann, 1992; Su et al., 1998). The crosses indicate the values used in the numerical simulations.

profile shown in Figure 2 was rescaled and used as a source for transpiration in the transport equation for q_t , and as a sink for photosynthesis in the equation for c_p .

3.2.1 LES validation

To validate our LES setup, we followed Su et al. (1998) and compared our numerical results with field experimental data from Shaw et al. (1988) over a sparse forest (LAI \approx 2). This simulation was neutral with a leaf-area density (LAD) and source profiles (only water vapor) as shown in Figure 2. In addition, the lower boundary condition for water vapor (i.e., q_e) was zero surface flux given the negligible evaporation at the experimental site.

A comparison between our LES results and the experimental data is included in the appendix (Figure B1). Along with the spatial statistics, we also show the temporal statistics computed as the ensemble average across the 24 towers in the domain. Good agreement is seen between spatially and temporally averaged results for all statistics. In particular, both spatial and temporal results for quadrant flux fractions (quadrant analyses) of momentum and water vapor are very similar and follow the experimental trends

383 well. In addition, while not directly used by the partitioning algorithms, the skewness
 384 of u and w using a dynamic drag model are in better agreement with observations than
 385 when a constant drag coefficient is used (comparison not shown here). Overall, we can
 386 conclude that the time series are converged and can be used for partitioning.

387 3.3 Simulating canopy openness

388 A homogeneous forest was first simulated by imposing a drag force and scalar sources/sinks
 389 at every horizontal grid point of the first 16 vertical levels. To investigate how the sparse-
 390 ness of the canopy influences the partitioning methods, we designed two new domains.
 391 The first domain replicates a vineyard (Figure 3) with rows oriented parallel to the y axis.
 392 The ratio of the width of the vegetation rows (r_v) to the width of the bare soil rows (r_s)
 393 is 0.81. The second domain is representative of a sparse orchard, where “clusters” of veg-
 394 etation of length $r_v \times r_v$ are separated horizontally from other clusters by a distance r_s .
 395 In both cases we kept the same canopy leaf-area density (LAI=2); thus, the effective leaf-
 396 area density is $LAI_e = LAI(A_v/A_t)$, where A_t is the total area of the xy plane and A_v
 397 is the area occupied by canopy elements. For the first and second domains, we thus have
 398 $LAI_e = 0.98$ and 0.42, respectively. In addition, the same canopy flux profiles and leaf-
 399 area density (Figure 2) were imposed. As boundary condition, we imposed a homoge-
 400 neous soil flux, *i.e.*, the same respiration and evaporation magnitudes being emitted from
 401 under the canopies, as well as from the exposed soil. Simulations with heterogeneous soil
 402 fluxes were tested, but are not shown here since the key conclusions remained the same.
 403 In addition, we found no sensitivity in the results based on the location of the towers (*i.e.*,
 404 vegetated grid cell versus a bare soil grid cell). The mean wind profile and kinetic en-
 405 ergy resultant from all three domains are shown in the Supplementary Information, sec-
 406 tion S1.

407 3.4 Implementation of partitioning methods

408 Following the simulation and sampling of time series, we implemented all partition-
 409 ing methods following the same steps as in field experiments. For FVS and CECw, we
 410 used the “real” water-use efficiency, which is imposed in the simulation. The flux com-
 411 ponents computed at every vertical grid point for all 24 towers were later averaged, re-
 412 sulting in one single profile for all four components and all four methods. As an exam-
 413 ple, the variability around the average values is illustrated in section S2 of the Supple-
 414 mentary Information. Note that not all towers yielded valid solutions at all levels for all
 415 methods; nonetheless, for each method, if at least one of the 24 towers converged to a
 416 valid solution at a height z , a valid estimate for this level is included in the plots. The rate
 417 of convergence to valid solutions, in particular for FVS, is discussed in the text.

418 As previously explained, our LES setup allows us to reconstruct the time series of
 419 c and q that would result from any combination of ET and F_c flux components. To in-
 420 vestigate as many combinations as possible — from stronger soil fluxes to fluxes dom-
 421 inated by canopy components — we linearly increased T/ET by increments of 0.025 from
 422 0.025 to 0.975, while keeping T constant. Similarly, the ratio P/RP , where we defined
 423 $RP = R + |P|$, was increased from -0.975 to -0.025 in increments of 0.025, as P was
 424 kept constant. Note that RP uses the absolute value of photosynthesis to ensure a ra-
 425 tio smaller than unity and no singularities when $P = -R$. Thus, the water-use efficiency
 426 remains the same for each of the 1600 flux combinations we generate.

427 The performance of each method was quantified by computing the biases of the canopy
 428 flux components. More specifically, we compute the bias of the flux ratios (T/ET and

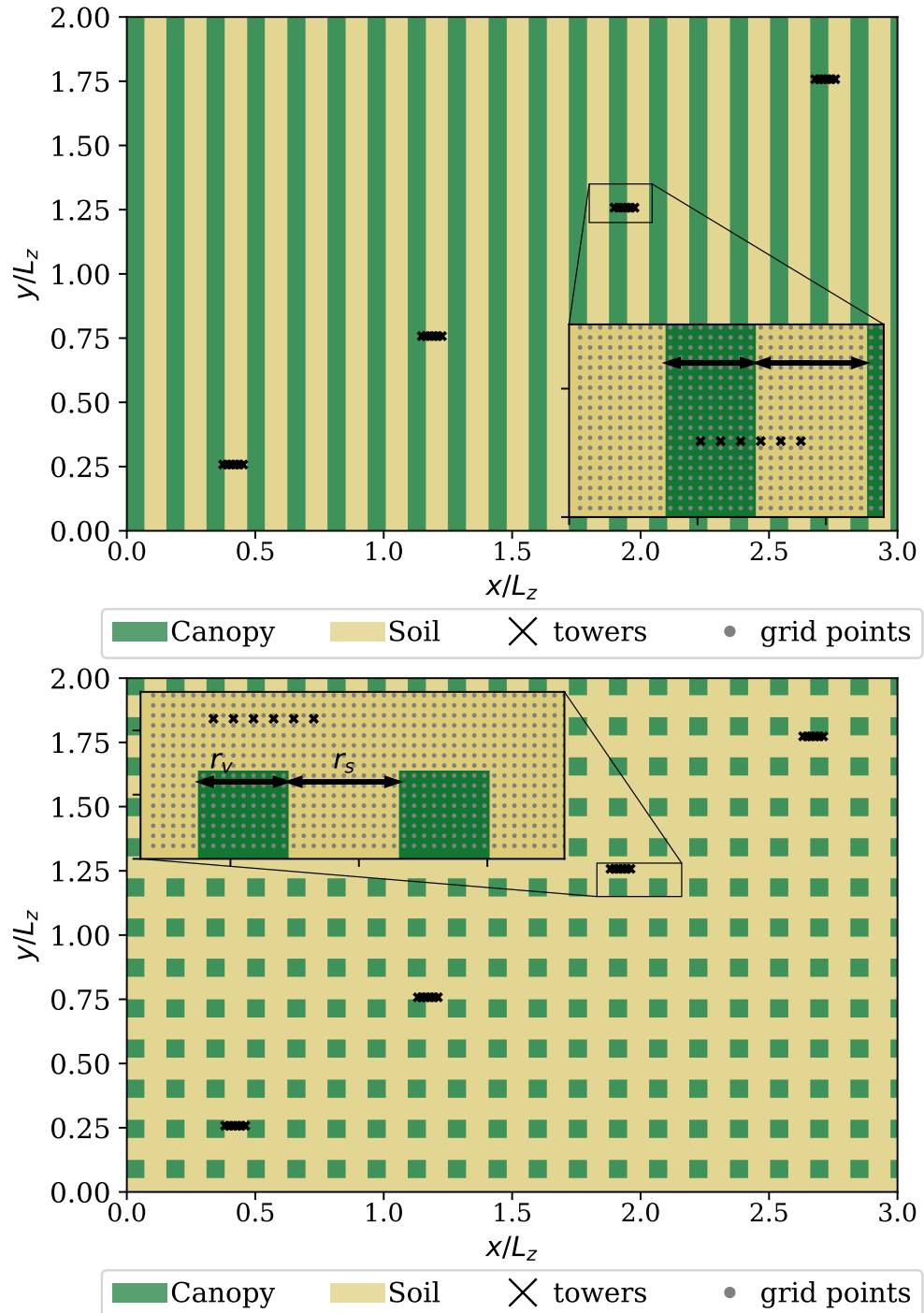


Figure 3. LES domain representing a vineyard (top) and clusters of trees (bottom).

429 P/RP) as follows,

430
$$\text{bias}_{T/ET} = \frac{T - T_{\text{part}}}{ET}, \quad (21)$$

431
$$\text{bias}_{P/RP} = \frac{P - P_{\text{part}}}{RP}, \quad (22)$$

432 where T and P are the imposed transpiration and photosynthesis fluxes that we wish
 433 to retrieve in the partitioning, while T_{part} and P_{part} are the flux components obtained
 434 by any of the four partitioning methods (FVS, CEC, CEA, and CECw). Note that we
 435 do not compute the absolute error of flux components because they do not represent the
 436 overall performance of each method. For instance, a 100% error in estimating T also de-
 437 pends on whether $T = 1 \text{ Wm}^{-2}$ and $E = 100 \text{ Wm}^{-2}$ (thus the error in E would be
 438 very small), or $T = 100 \text{ Wm}^{-2}$ and $E = 1 \text{ Wm}^{-2}$. Since our analysis covers various
 439 flux combinations, the bias of the flux ratios are more appropriate.

440 **4 Assessing the Performance of the Four Methods**

441 We start this section by discussing the impact of canopy sparseness on transport
 442 efficiency; in particular, how the presence of gaps, or “canyons”, influence turbulence mix-
 443 ing, and what are the implications for flux partitioning. We follow by investigating the
 444 performance of each partitioning method for different measurement heights, flux com-
 445 ponent strength combinations, and canopy sparseness.

446 **4.1 Effect of canopy sparseness on mixing efficiency**

447 A common feature across all four partitioning methods is their requirement of a
 448 degree of uncorrelatedness between soil and plant flux components: the parcels emanat-
 449 ing from the soil and plants cannot be well mixed (correlated) if the separate signals are
 450 to be captured. The CEC, CEA, and CECw methods further require the presence of ed-
 451 dies that were in contact with the soil, and were subsequently transported to the sen-
 452 sor level without being fully mixed. Therefore, one expects that plant canopies with ex-
 453 posed gaps, such as vineyards, would offer a suitable environment for these methods. To
 454 explore the differences in turbulent statistics in different plant canopy configurations, we
 455 show in Figure 4 the correlation coefficient between c_r and c_p , namely ρ_{c_p, c_r} , as well as
 456 the skewness (Sk_{c_p} and Sk_{c_r}) of both quantities obtained from simulations over a ho-
 457 mogeneous canopy, a vineyard, and a cluster domain. Note that ρ_{c_p, c_r} is here used as
 458 a measure of the degree of mixing between soil and canopy air parcels; for instance, in
 459 the event when $\rho_{c_p, c_r} = -1$, the parcels are fully mixed and no relevant partitioning
 460 information can be extracted. Identical conclusions can be made from the statistics of
 461 q_e and q_t , which are thus not included.

462 As shown in Figure 4a, the correlation between soil and plant components approaches
 463 -1 faster, as the height increases, above the vineyard and the cluster domains. The im-
 464 plication is that soil respiration is mixed faster and at a lower height above the soil when
 465 wide gaps between plants are present. This, it turns out, is due to stronger shear tur-
 466 bulence generation by the gaps, compared to the homogeneous setup. Therefore, ejec-
 467 tions enriched in CO_2 , representing the soil surface, are more likely to be sampled be-
 468 fore being fully mixed into the flow over the homogeneous canopy. Figure 4b further cor-
 469 roborates this argument by indicating greater skewness for c_r in the homogeneous do-
 470 main at $z/h < 2$. In this case, greater skewness indicates that more parcels were sam-
 471 pled with high c_r values as a result of ejections carrying parcels enriched in CO_2 . Fig-
 472 ure 4b also indicates that scalars emitted by the canopy distributed profile have smaller
 473 skewness magnitudes than the scalar emitted at ground level due to stronger mixing in-
 474 side the canopy. These results are in agreement with Edburg et al. (2012)’s findings, in-
 475 dicating that strong and intermittent organized turbulence structures penetrate the en-
 476 tire canopy, albeit infrequently, causing bursts of scalars emitted from the soil.

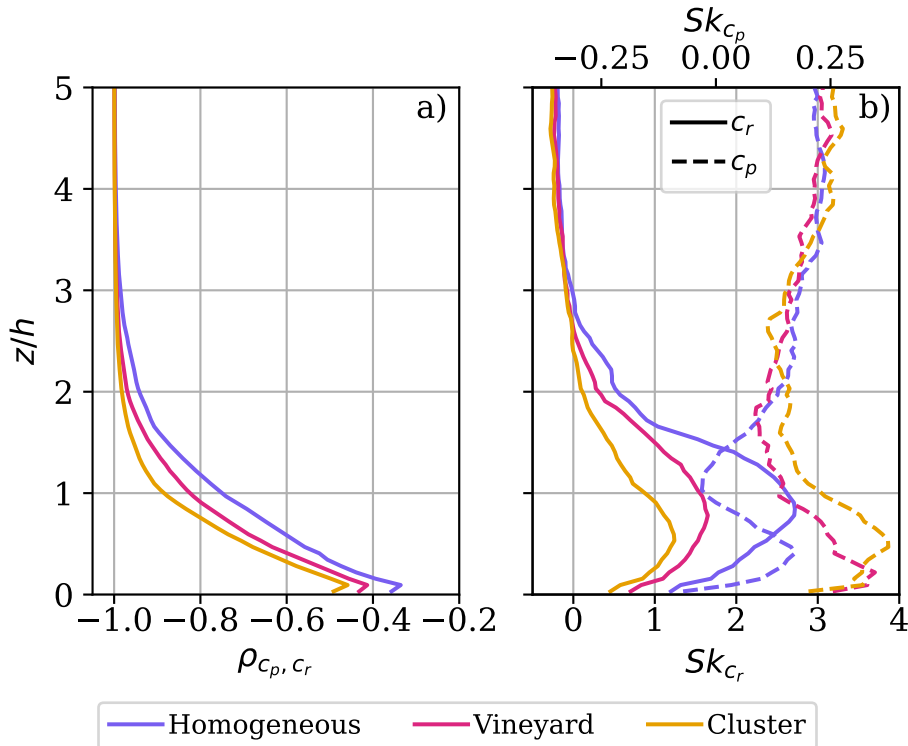


Figure 4. Correlation between soil and plant components, and their individual skewness, over homogeneous and heterogeneous canopies. Note that part (b) has a top and bottom x -axes.

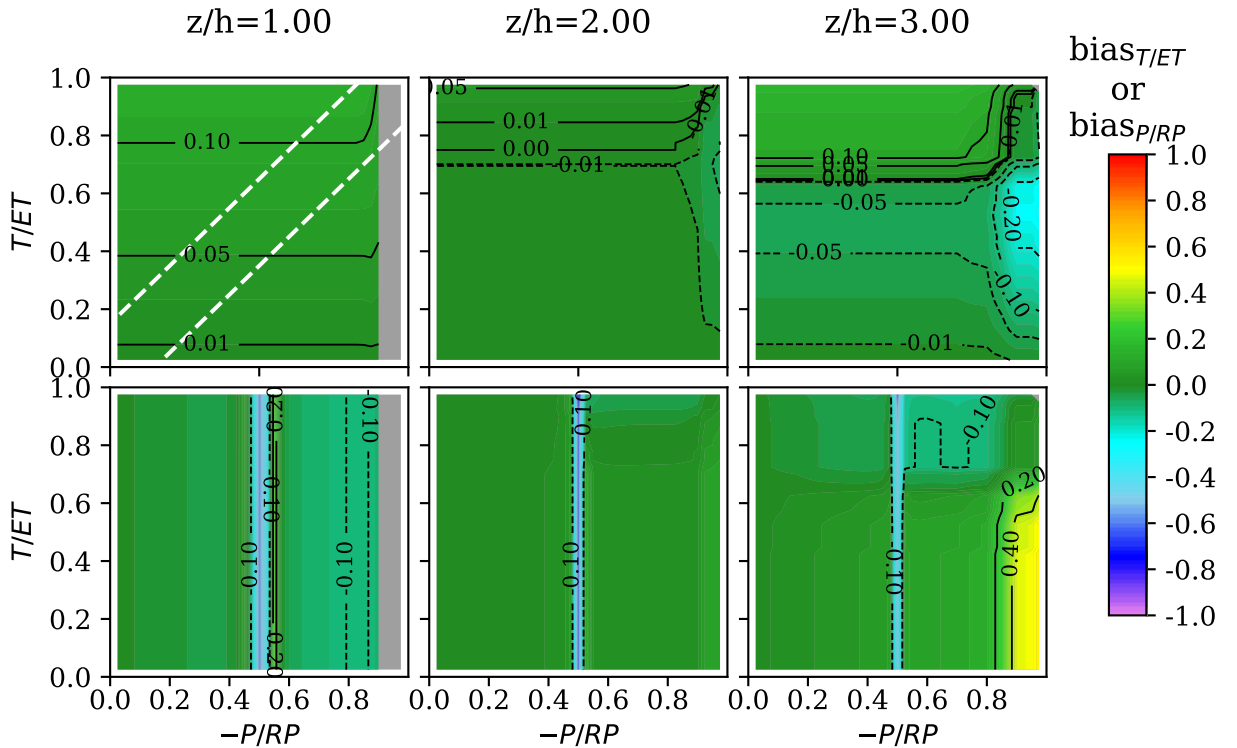
Overall, these results contradict our initial expectation that exposed patches of soil improve the representativeness of soil respiration in conditional sampling analyses. In fact, they indicate that the opposite is true, *i.e.*, that the presence of wide gaps (or canyons) increases turbulence mixing of soil fluxes, potentially worsening the performance of FVS, CEC, CECw, and CEA. Nonetheless, while vegetated canopies with the presence of open canyons and gaps are non-ideal, it is still necessary that the vegetated canopy of interest be porous enough such that updrafts originating below the canopy can escape vertically. As discussed by Zahn et al. (2022), canopies that are too dense might lead to uncoupled flows and lateral advection of soil fluxes (Thomas et al., 2013) that are not only problematic to partitioning, but to flux quantification in general.

4.2 Partitioning versus flux component strength at various elevations

In this section, we explore the performance of all four partitioning methods evaluated with regards to measurement height and the relative magnitude of plant and soil fluxes of CO_2 and H_2O . As expected based on the comparison of mixing efficiency across domains — indicating faster mixing of soil and canopy scalars when large gaps are present — the partitioning performance for both heterogeneous domains is slightly worse than those over the homogeneous case. Thus, we will focus on the results for the homogeneous canopy simulation, noting that the figures for both heterogeneous domains are included in the supplementary information in sections S3 and S4.

4.2.1 FVS

497 The biases in the partitioning computed by the FVS method are shown in Figure
 498 5. These results clearly indicate that, as long as the water-use efficiency is known exactly
 499 and the method converges to a solution, the FVS method has an excellent performance
 500 partitioning ET and CO_2 across most flux magnitude combinations. Nonetheless, larger
 501 errors or no physically-valid solution were observed more often when the correlation be-
 502 between c and q , $\rho_{c,q}$, approached unity. In Figure 5, this corresponds to conditions when
 503 photosynthesis dominates the total CO_2 flux ($-P/RP > 0.8$ in the figure). This be-
 504 havior was even more evident above the cluster domain (S4.1 of the SI) and at higher
 505 levels, where stronger mixing increased $\rho_{c,q}$. A more detailed discussion on the role of
 506 scalar mixing on the FVS assumptions is addressed in section 5.1.



507 **Figure 5.** The top three plots show the bias in the partitioning of ET following the FVS
 508 method at $z/h = 1, 2, 3$, where the colors represent the bias in transpiration, $(T - T_{FVS})/ET$.
 509 Bottom plots show the bias for CO_2 components, defined as $(P - P_{FVS})/RP$, where $RP = R + |P|$.
 510 Regions in gray represent combinations where no physical solutions were found in any
 511 of the 24 towers. Flux combinations inside the area delimited by the white dashed lines represent
 512 the condition $-P/RP - 0.15 < T/ET < -P/RP + 0.15$, from which we will later select points for
 513 further analysis. Colorbar spans ± 1 for easy comparison with subsequent figures.

507 4.2.2 CEC

508 The bias with regard to the correct ratio T/ET (top panel) and R/RP (bottom
 509 panel) obtained by the CEC method is shown in Figure 6. Focusing on $z/h = 1$, we
 510 can identify a region along the diagonal with $|(T - T_{CEC})|/ET \leq 0.2$, indicating smaller
 511 biases for ET . In particular, we see that the best agreement is expected when the ra-
 512 tios $-P/R$ and T/E grow in tandem. On the other hand, greater errors are expected
 513 when one component overwhelmingly dominates the other. Thus, one requirement for

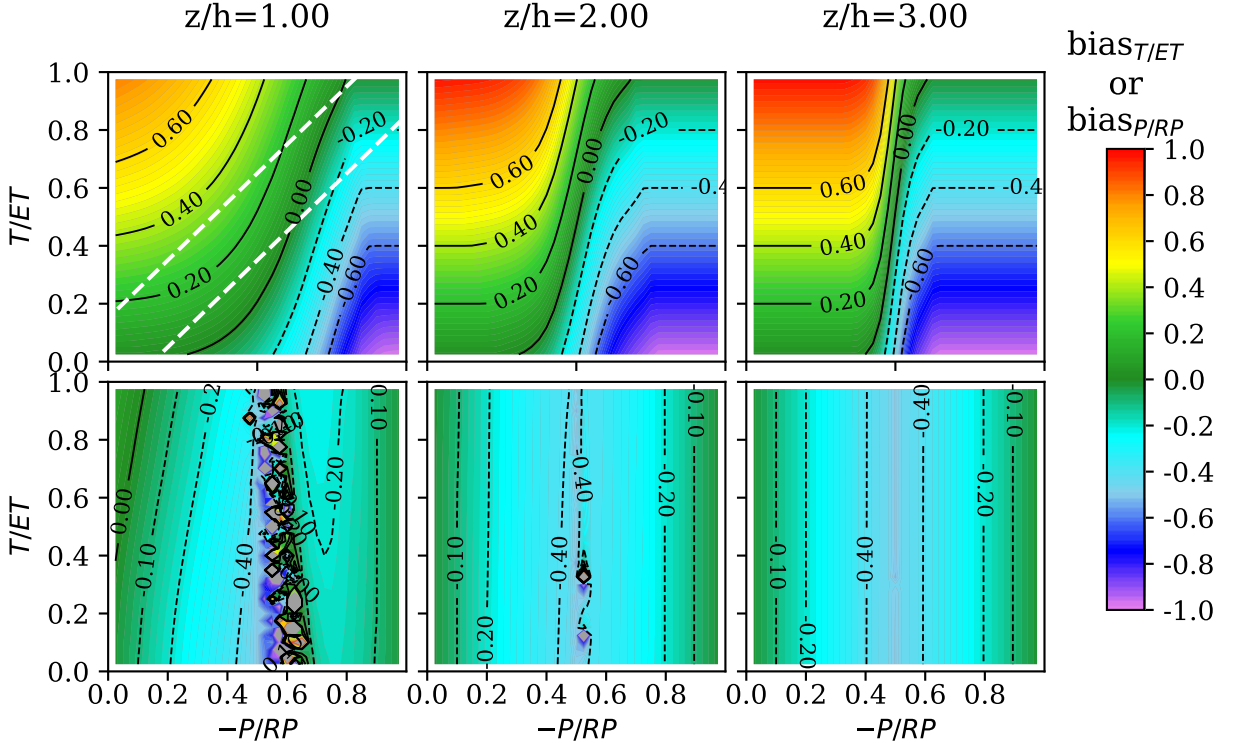


Figure 6. Same as 5, but for the CEC method.

good performance of CEC is that the ratios P/T and R/E should not be too dissimilar. However, note that regions where $|(T - T_{CEC})|/ET \geq 0.2$ correspond to flux combinations that are unusual or physically improbable. For instance, the top left corner would indicate fluxes dominated by transpiration and respiration, but with little evaporation and photosynthesis. Such occurrence is unlikely given the expected proportionality between transpiration and carbon assimilation as defined by the water-use efficiency. Soil components, on the other hand, share physical drivers such as soil moisture and temperature, as well as turbulence intensity near the surface, but they are more loosely coupled compared to their canopy counterparts. After rain, for instance, it is possible that respiration could be suppressed by soil saturation (Xu et al., 2004), while evaporation would be large.

The accuracy of CO_2 partitioning using CEC is not as precise as for ET , as illustrated in the bottom panel (particularly at $-P/RP \approx 0.5$ when the carbon fluxes exactly cancel, region where the FVS predictions were also poorer). This discrepancy mainly arises from the unbounded combination of components P and R in recovering the correct F_c . Unlike ET , which is constrained by the sum of E and T , the absence of additional constraints for F_c is a challenge for all partitioning methods that do not use additional inputs such as the water-use efficiency. However, it is important to note that this limitation does not affect ET partitioning. In this case, the primary function of CO_2 is to serve as a tracer for identifying the source of water vapor. Therefore, even if CEC cannot detect the correct magnitude of P or R , it can still leverage the sign of the CO_2 fluxes to detect if water vapor is coming from the canopy or from the soil.

As we move to higher levels, the region where $|(T - T_{CEC})|/ET \leq 0.2$ becomes narrower, and good performance for CEC in partitioning water vapor flux is confined to cases when R is on the order of $-P$ or much larger than P , with the obvious excep-

539 when $R = -P$. These results corroborate previous experimental findings (Zahn
 540 et al., 2022) suggesting that the best performance of the CEC method is achieved for
 541 measurements collected as close to the canopy as possible, ensuring that some uncorre-
 542 latedness between the various sinks and sources is sampled.

543 **4.2.3 CEA**

544 Results for the CEA method are moderately superior, but broadly similar, to CEC
 545 at the homogeneous canopy (Figure 7), as well as above the vineyard and cluster domains
 546 (section S3 and S4 of the SI). The biases for ET partitioning are lower, and CEA out-
 547 performs CEC significantly at higher levels. Similarly, larger errors for ET partitioning
 548 were observed usually for unrealistic flux combinations, for the same reason as CEC. An-
 549 other similarity with the CEC method is the less precise results for F_c partitioning: while
 550 the method may not accurately identify the correct magnitudes, CEA also can utilize
 551 the turbulent transport of CO_2 and the sign of c' to determine the magnitude of ET flux
 552 components.

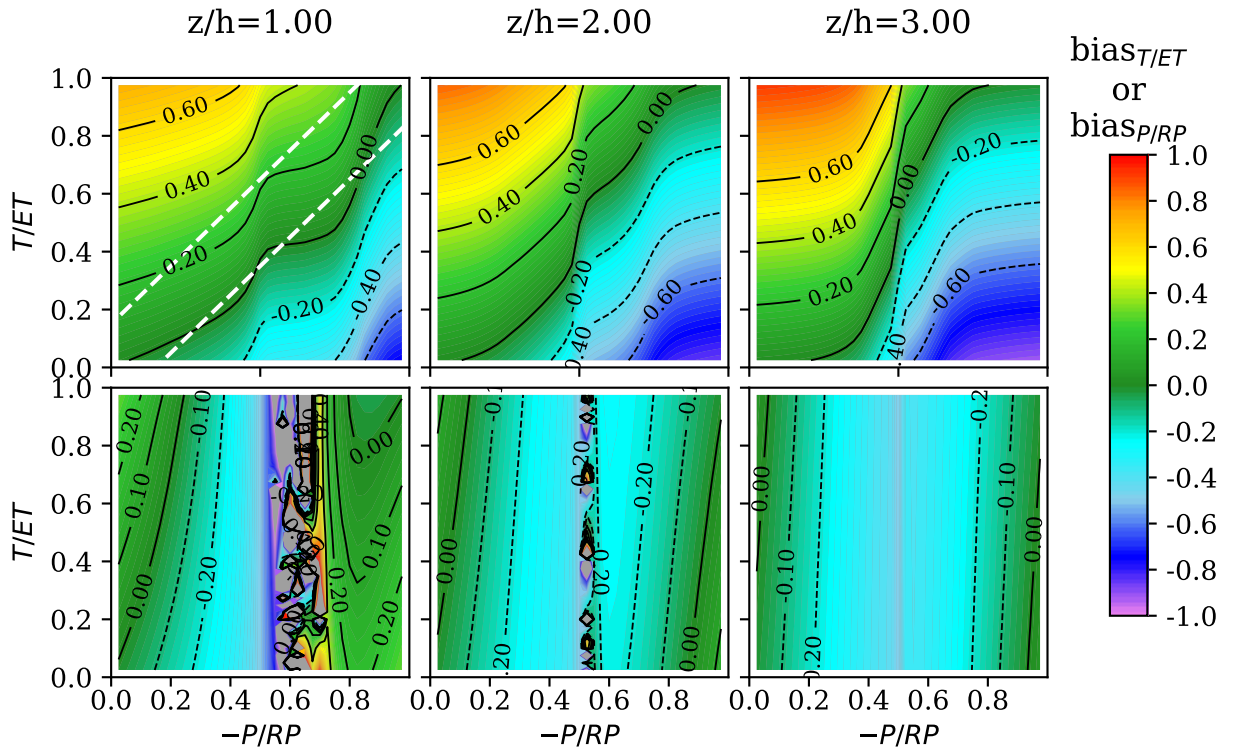


Figure 7. Same as 5, but for the CEA method.

553 **4.2.4 CECw**

554 Lastly, we show the results obtained with the CECw method. Interestingly, despite
 555 similar assumptions to CEC, it performs better than the former in partitioning ET and
 556 F_c , displaying a wider range where biases are smaller than 20% and consistent perfor-
 557 mance at least up to $z/h = 3$. Furthermore, its performance in partitioning F_c is also
 558 quite different from CEC or CEA, with much better performance along the 1:1 diag-
 559 onal. The improvement in CO_2 partitioning is a direct result of the input of water-use
 560 efficiency, which now helps constraint the magnitude of P and R . Thus, these superior

561 results are dependent on prior knowledge of the water-use efficiency, and the performance
 562 of the CECw method share this shortcoming (and the advantages if W is known) with
 563 the FVS method.

564 In addition, although not performing as well as FVS when W is known, the CECw
 565 method is easier to implement and its poor performance, e.g. where $(T-T_{CECw})/ET \geq$
 566 ± 0.2 , is restricted to regions with unlikely flux combinations as with CEC and CEA.
 567 Comparing regions where CECw and FVS do not find valid solutions (gray zones in fig-
 568 ures 5 and 8), we see that generally they do not overlap, in particular for ET partition-
 569 ing. Thus, CECw seems to be a good complement to the FVS method, ensuring a com-
 570 plete record of flux components that are consistent with the water-use efficiency that both
 571 methods require. Yet, the resulting complete record will also be subject to the uncer-
 572 tainty that propagates from the uncertainty in W .

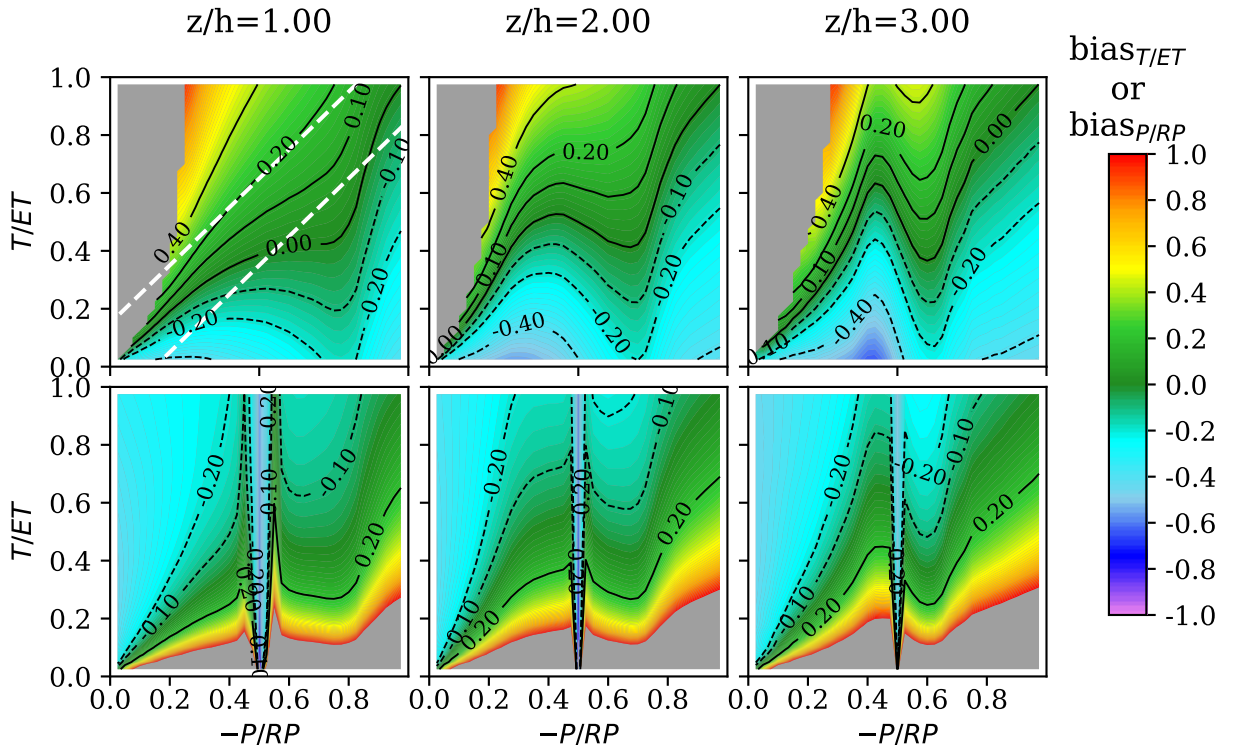


Figure 8. Same as 5, but for the CECw method.

573 5 Probing some Underlying Physical Assumptions

574 One of the main advantages of investigating the partitioning methods through nu-
 575 matical simulations is the possibility of assessing their physical and mathematical assump-
 576 tions. By simulating all four scalars separately, we investigate in the next subsection if
 577 the approximations adopted by Scanlon and Sahu (2008) and Scanlon and Kustas (2010)
 578 in their mathematical derivation are robust. We then examine the ability to distinguish
 579 eddies emanating from the soil and plants, invoked for both CEC, CECw and CEA. This
 580 section ends with an evaluation of how errors in the estimate of the water use efficiency
 581 degrade the performance of FVS and CECw.

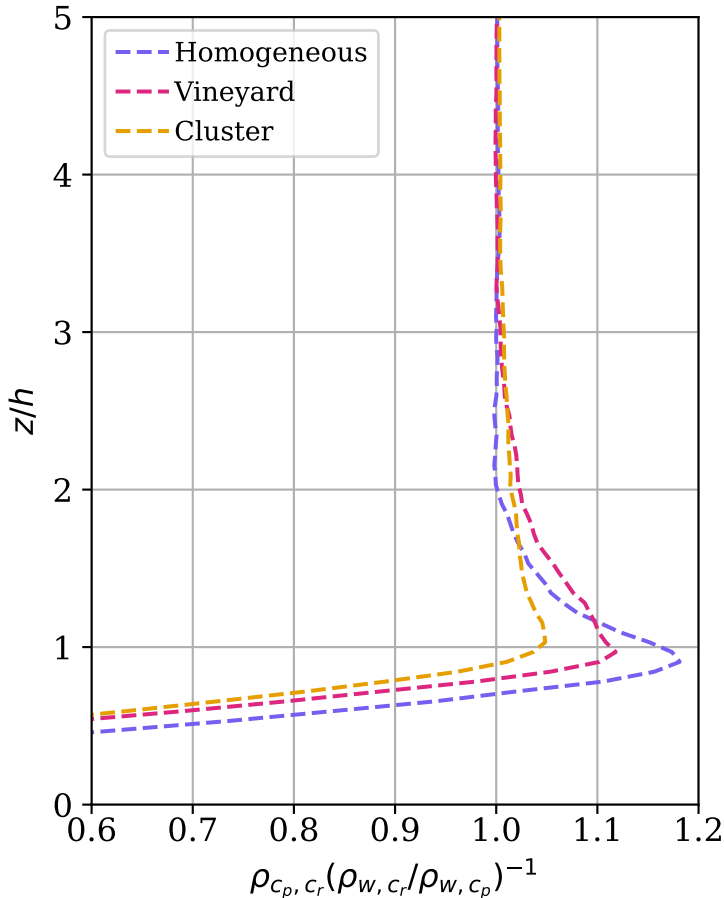


Figure 9. Profile of the ratio defined by equation (1). When this ratio reaches unity, it indicates that the approximation is valid. Profiles were obtained by averaging the correlation coefficients at each level across all 24 towers.

582 5.1 Assumptions and uncertainties of the FVS method

583 The expressions given by equation (1) represent the main source of uncertainty in
 584 the FVS method (not considering the ability to estimate W). These approximations as-
 585 sume that the correlation coefficient between plant and soil CO_2 (ρ_{c_p, c_r}) can be estimated
 586 as the ratio of their respective transfer efficiencies ($\rho_{w, c_p}/\rho_{w, c_r}$), the same applying to
 587 H_2O components. Such approximation was first proposed by Katul et al. (1995) in their
 588 study of similarity between temperature and water vapor. Bink and Meesters (1997) later
 589 demonstrated that $\rho_{T,q} \approx \rho_{w,T}/\rho_{w,q}$ can yield satisfactory results as long as $\rho_{w,T} <$
 590 $\rho_{w,q}$, that is, when water vapor is more efficiently transported by turbulence than tem-
 591 perature; if the opposite is true ($\rho_{w,T} > \rho_{w,q}$), then the appropriate approximation is
 592 $\rho_{T,q} \approx (\rho_{w,T}/\rho_{w,q})^{-1}$.

593 Following the arguments of Bink and Meesters (1997), Scanlon and Sahu (2008)
 594 assumed that the transfer efficiency of plant components, c_p and q_t , are greater than the
 595 transfer efficiency of soil components, c_r and q_e , due to data sampling being done above
 596 the canopy (i.e., close to the sink of c_p and q_t). Thus, for c we need to satisfy $\rho_{w,c_p} >$
 597 ρ_{w,c_r} , which clearly satisfies $|\rho_{c_p, c_r}| \leq 1$.

598 Figure 9 shows how this approximation (a value of 1 in the plot implying zero error)
 599 holds over a homogeneous canopy, as well as for the two sparse canopies described
 600 in 3.2. Results for CO₂ and H₂O are the same, thus only the former are shown. In ad-
 601 dition, note that these results do not depend on the magnitude of soil and canopy fluxes,
 602 meaning that the same results hold regardless of the magnitude of respiration (evapo-
 603 ration) and photosynthesis (transpiration). Overall, it is clear that the approximation
 604 is worse below the canopy top where the transfer efficiency of respiration is greater given
 605 the proximity to the soil. Above the canopy, on the other hand, the approximation is
 606 more appropriate, almost reaching equality. In addition, the faster convergence towards
 607 unity in sparser canopies is a consequence of the more efficient turbulent mixing in the
 608 presence of gaps, as previously discussed.

609 For $z/h \geq 3$, the magnitudes of the correlation ρ_{c_p, c_r} — as well as ρ_{q_t, q_e} and $\rho_{c, q}$
 610 (not shown in the figure) — reach values close to unity for all three domains, causing
 611 the approximation in Equation (1) to approach equality. However, the derivation of the
 612 FVS method requires $|\rho_{c, q}| < 1$ (see equation 5), *i.e.*, it is undefined in case of perfect
 613 correlation. Therefore, on one hand FVS requires a degree of decorrelation between scalars;
 614 on the other hand, its mathematical approximations in equation (1) are more accurate
 615 in regions where the different scalars are better mixed and their correlations are almost
 616 perfect. These contradictory requirements, also observed by Klosterhalfen, Moene, et al.
 617 (2019), add complexity to the interpretation of field data partitioning using FVS, and
 618 potentially decrease the number of valid partitioning estimates. This is illustrated in Fig-
 619 ure S5.1 of the SI, which shows that less valid solutions are found across towers at *i*) higher
 620 levels, *ii*) over open canopies (vineyard setup for instance), and *iii*) when P dominates
 621 the total CO₂ fluxes, all conditions when scalar correlation was found to converge to-
 622 wards ± 1 .

623 A different approach to guarantee equality of expression (1) would be its multipli-
 624 cation by a correction factor, as done by Klosterhalfen, Moene, et al. (2019). Nonethe-
 625 less, as shown by the authors, the correction values obtained from their simulations vary,
 626 and the extrapolation to real field data is impractical. Thus, we do not pursue this cor-
 627 rection here. With the limited information we usually have from experimental data, we
 628 can only hypothesize that a measurement height where there is strong, but not complete,
 629 mixing is preferable for the FVS method, and should result in the smallest uncertain-
 630 ties with regards to (1).

631 5.2 Investigating the conditional sampling of eddies from the canopy and 632 from the soil

633 The main assumption behind the CEC, CECw and CEA methods is that, consid-
 634 ering that the measurements are done close enough to the sinks and sources, we are able
 635 to distinguish turbulent structures coming from the soil or from the canopy. To inves-
 636 tigate if this assumption is appropriate, we show in Figure 10 instantaneous snapshots
 637 of c'_r , c'_p , and the total CO₂, c' , simulated for a homogeneous domain.

638 The snapshot of c_r in Figure 10d clearly shows the presence of turbulent structures
 639 enriched in CO₂ right above the surface (see for instance, $x/L_z \approx 1.5, 2.4$). These same
 640 structures persist — although with smaller concentration given the assimilation of CO₂
 641 — in the reconstructed field of total c in Figure 10f. Similarly, we can observe regions
 642 depleted in CO₂ as a result of assimilation (e.g., $z/L_z \approx 3.0$ in Figure 10e) and that
 643 are still present in the field of total CO₂. These results thus lend credibility to the as-
 644 sumption that we can distinguish the origin of eddies solely based on high-frequency mea-
 645 surements. More specifically, CO₂ can indeed be utilized as a tracer to detect the ori-
 646 gin of flux events for carbon as well as water vapor. However, note that these structures
 647 are only distinguishable below $z/h = 3$ (white dashed line); above that level, turbulent
 648 mixing becomes stronger and we are no longer able to separate plant and soil signals.

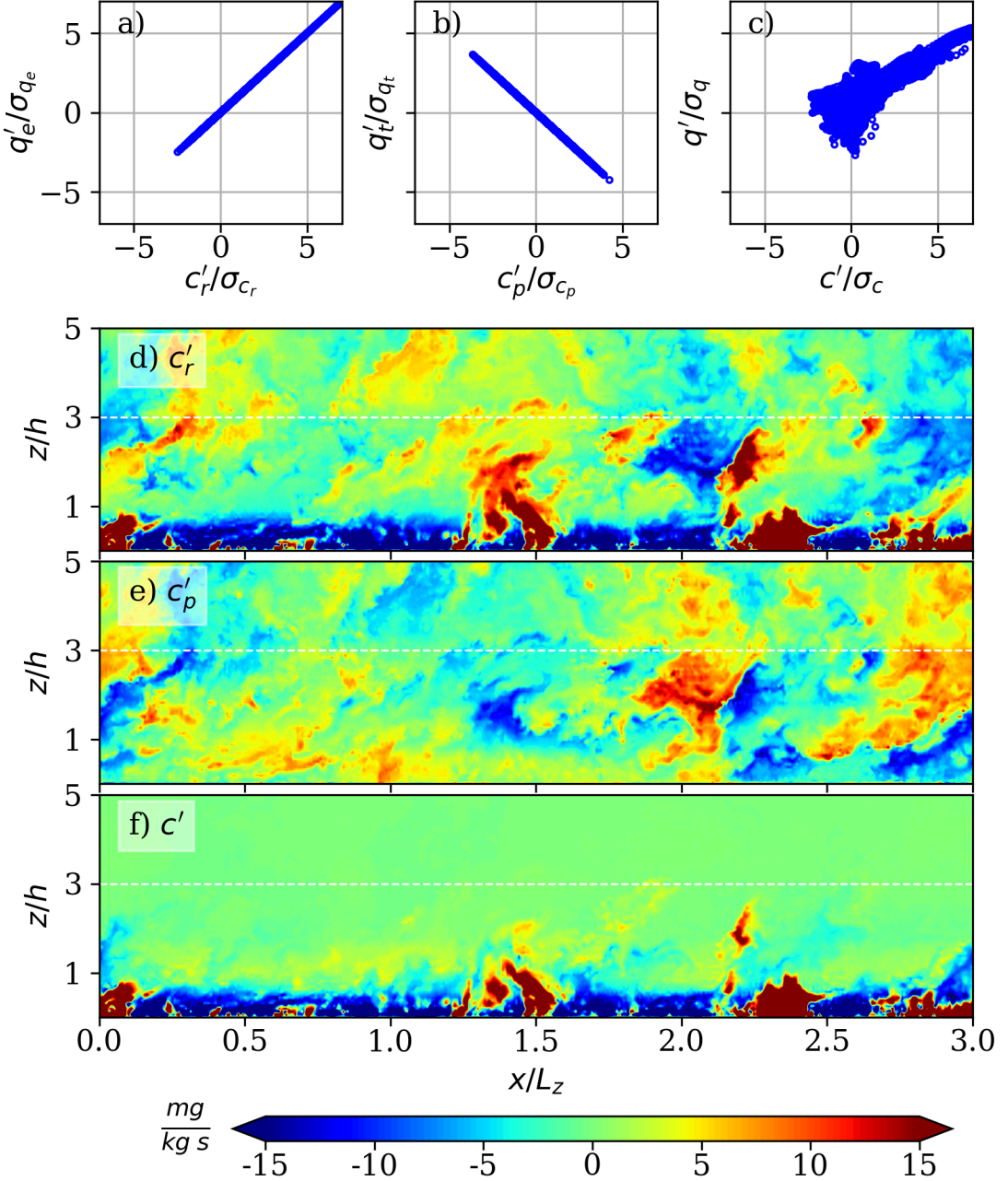


Figure 10. Panels a-c show the quadrant plot between the different components of c and q from a time series measured at $z/h \approx 1.2$. Only ejections ($w' > 0$) are included. Note that the conditional sampling implemented by the CEC is based on plot c). The bottom three panels show instantaneous fields of d) c'_r , e) c'_p , and (f) $c' = c'_r + c'_p$. The white dashed line represents the height $z = 3h$. In this neutral simulation over a homogeneous canopy, $R = -P = 1 \text{ mg m}^{-2} \text{s}^{-1}$.

649
650

This corroborates the decreased performance of these methods reported in the previous section at higher elevations. The findings also support previous conclusions (Zahn et al.,

651 2022) that CEC, and this also applies to CEA and CECw, is more likely to perform better
 652 when sampling is done as close as possible to the canopy top.

653 In Figures 10a–c we show an example of the quadrant analyses of a time series measured
 654 at $z/h = 1.2$. Points on the first quadrant — related to respiration ($w' > 0, c' > 0, q' > 0$) — have larger concentrations than on the second ($w' > 0, c' < 0, q' > 0$),
 655 which is related to photosynthesis. This asymmetry — evident in the skewness profile
 656 shown in Figure 4 — is caused by stronger bursts of parcels enriched in CO_2 that were
 657 “trapped” under the canopy and took longer to be ejected. Carbon assimilation, on the
 658 other hand, is the strongest at the top of the canopy (Figure 2), and thus air parcels de-
 659 pleted in CO_2 located around $z/h \approx 1$ are mixed faster. Despite the asymmetry, the
 660 quadrant plot of c shows that conditional sampling is able to distinguish between the con-
 661 tribution of soil and canopy eddies, and can thus be used to infer the conditional flux
 662 ratios (equation 8).

663 The main difference observed in the patterns over homogeneous and heterogeneous
 664 domains (vineyard and cluster, section S6 the SI) is the blending height at which full mix-
 665 ing of flux components happens. As expected from the greater turbulent mixing efficiency
 666 in sparser canopies, ejections carrying the soil signature are shorter lived, being almost
 667 fully mixed with the flow above $z > 2h$; for the cluster-like domain these structures are
 668 only distinguishable below $z < h$. These results suggest that in very open canopies, the
 669 measurement height should be even closer to the canopy, ideally at the canopy top, to
 670 ensure the best performance possible for CEC and CEA. It is important to note that bet-
 671 ter total flux convergence is expected away from the canopy at a height of at least 1.4
 672 h (Pattey et al., 2006), where the wakes and signatures of individual plants are erased.
 673 To avoid loss of information caused by EC measurements close to the canopy top (both
 674 for homogeneous and heterogeneous configurations), one approach would be the sim-
 675 taneous placement of an EC system at $z \approx h$, which will be used to estimate the flux
 676 ratios (E/T and R/P), and one system further away from the effects of the canopy layer
 677 ($z > 1.4h$). By considering that the flux ratios measured at the canopy top are con-
 678 served, we can use this information to obtain converged flux components further away
 679 from the canopy.

681 5.3 Sensitivity of FVS and CECw to water-use efficiency

682 As shown in previous sections, the FVS and CECw methods are reliable partition-
 683 ing approaches when the water-use efficiency is known. However, such information is usu-
 684 ally not available from measurements, and different parameterizations of W have shown
 685 to result in large variability (Skaggs et al., 2018; Zahn et al., 2022).

686 To illustrate how the sensitivity of these methods to W vary with different flux mag-
 687 nitude combinations, we plot a phase diagram for biases in T and P (at $z/h = 1$) for
 688 different cases when W is overestimated or underestimated. Here, the water-use efficiency
 689 given to both methods, W_{input} , was increased by up to 2 times or reduced to 0.5 times
 690 its original value, W_{real} , used in LES to generate the time series. This range was selected
 691 based on the variability detected for W using different parameterizations (Zahn et al.,
 692 2022; Wagle et al., 2020) and thus represent uncertainties expected in field experiments,
 693 noting that the variability across models can be more than two orders of magnitude and
 694 depend on the time of the day (Wagle et al., 2021).

695 Results for FVS and CECw are shown in Figures 11 and 12. Less solutions are found
 696 by both methods when W is underestimated to half of the original value ($W_{\text{input}} = 0.5W_{\text{real}}$)
 697 than when it is overestimated by 100% ($W_{\text{input}} = 2W_{\text{real}}$). For FVS, it is also clear that
 698 larger errors are expected when plant components dominate (upper right corners in Fig-
 699 ures 11a and 11d) regardless of whether W_{input} was over or underestimated. Overall, this
 700 analysis suggests that the sensitivity of both methods to W is influenced not only by its
 701 accuracy but also by the combination of the four flux components. While this study fo-

702 cused on measurements at the top of the canopy, the lack of valid physical solutions may
 703 increase at higher canopy levels due to stronger scalar correlation. Nevertheless, these
 704 findings underscore the importance of improving measurements or parameterizations of
 705 W , as well as characterizing its uncertainty, to enable wider and more accurate appli-
 706 cation of FVS and CECw.

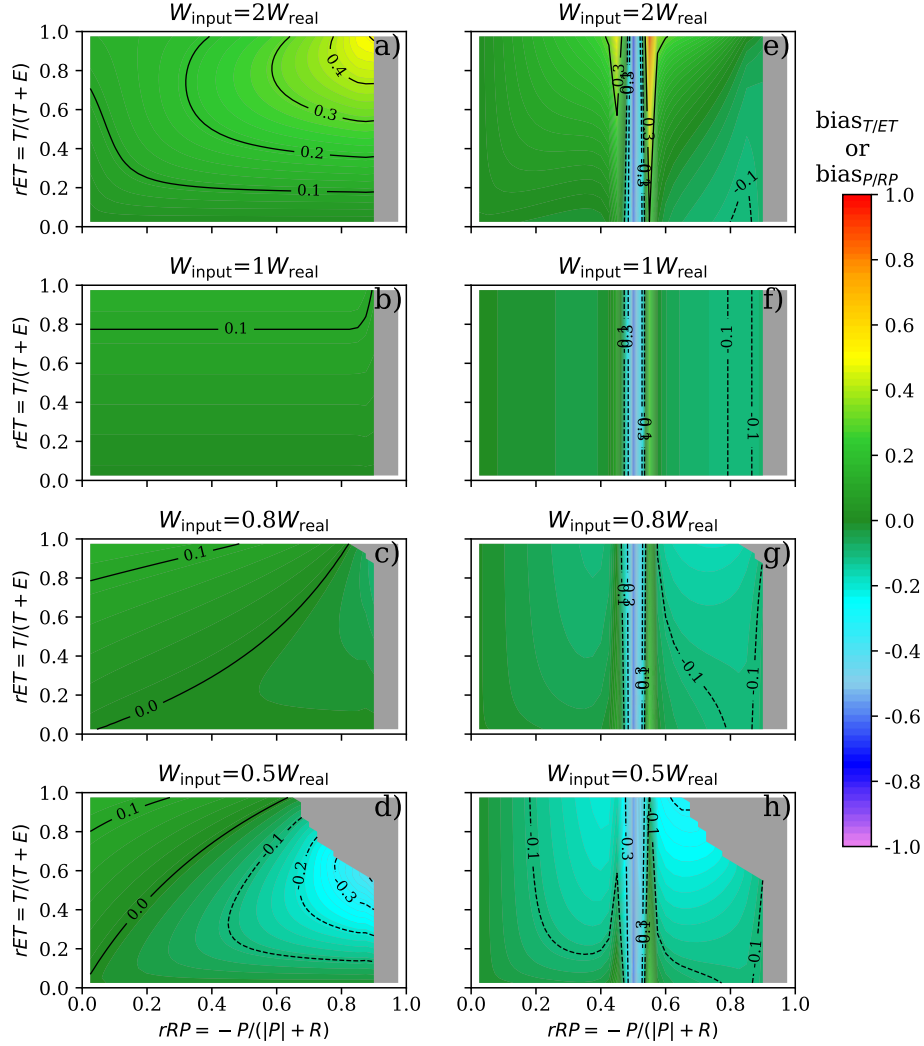


Figure 11. Phase diagrams indicating the sensitivity of the FVS method to uncertainties in the water-use efficiency at $z/h = 1$. $\text{bias}_{T/ET}$ is shown on the left side (plots a)–d), while $\text{bias}_{P/RP}$ is shown on the right side (plots e)–h). Regions in gray indicates conditions when no physical solutions were found.

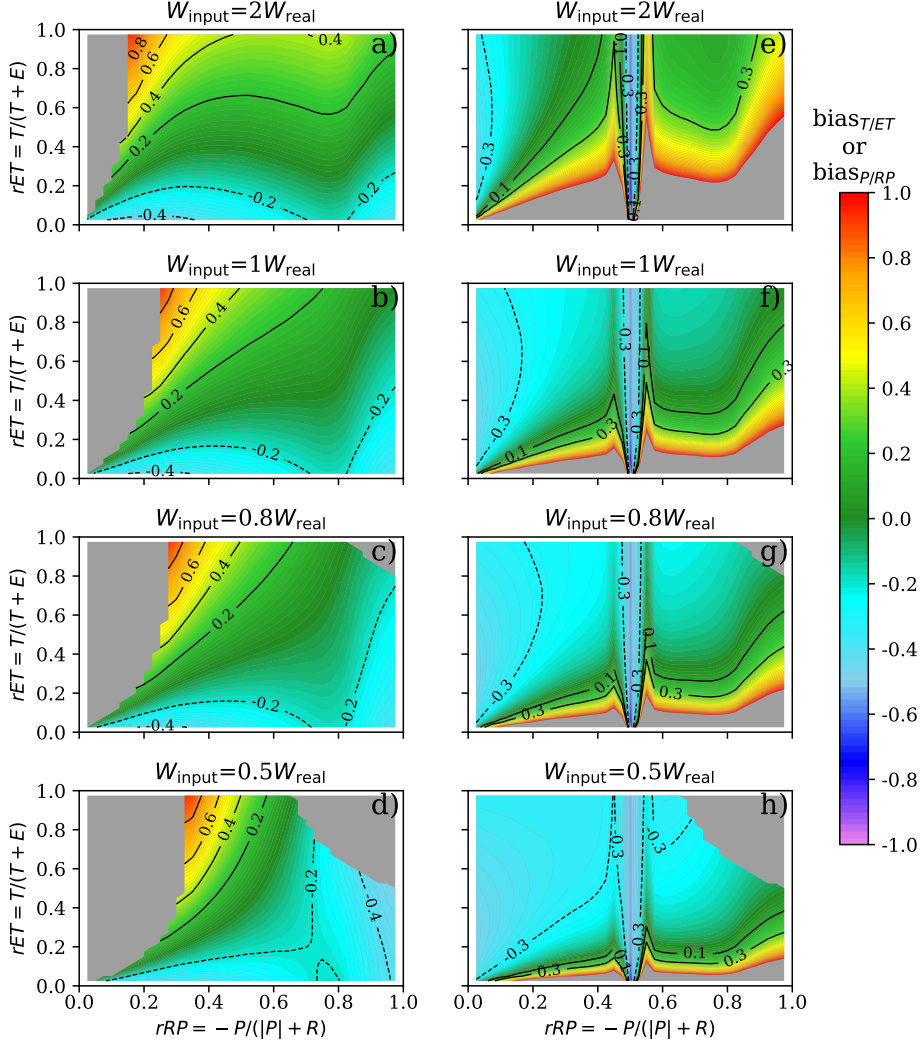


Figure 12. Same as Figure 11, but for the CECw method.

6 Connecting Biophysiological Variables to Turbulence Statistics

In this section, we explore the connection between the water-use efficiency, as imposed in our simulations, and the correlation coefficient $\rho_{c,q}$ retrieved from the final simulated turbulence data. Figure 13a shows the variation of W/W_f , where we defined a “total” flux water-use efficiency $W_f = F_c/ET$, with $\rho_{c,q}$ at four heights above the canopy. In addition, for all heights, we only show flux component combinations presented on the phase diagrams when $-P/RP - 0.15 < T/ET < -P/RP + 0.15$ (see dashed lines in the first plot of Figure 5). This constraint not only selects periods when all methods performed well, but also removes the most “unphysical” or rare flux component combinations.

First we note that $W/W_f = (1 + E/T)(1 - R/P)^{-1}$; therefore, $W/W_f > 0$ implies $R < |P|$ while $W/W_f < 0$ implies $R > |P|$. A stronger connection between $W/W_f > 0$ and $\rho_{c,q}$ is noticed at the top of the canopy, with W/W_f increasing as the correlation increases from -1 to ≈ 0.5 . The same trend is still visible at $z/h = 2$, although it is less “continuous”, with the presence of “gaps”, as we go above this level. Overall, for $W/W_f >$

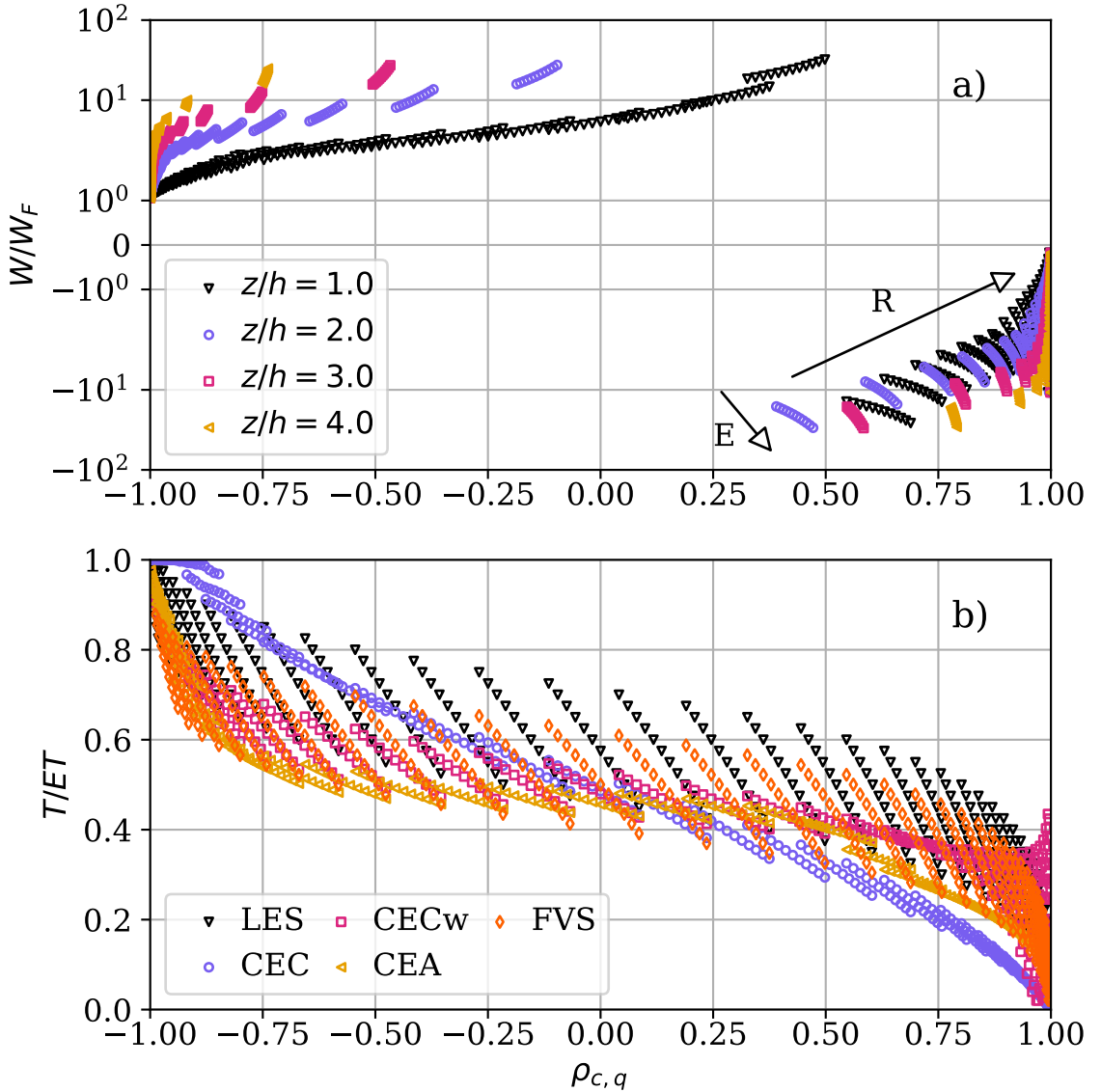


Figure 13. Panel (a) shows the relation between the ratio W/W_f and $\rho_{c,q}$ at heights $z/h = 1, 2, 3, 4$, where $W = P/ET$ and $W_f = F_c/ET$ were computed from the imposed (“true”) flux components. Panel (b) shows the ratio T/ET versus $\rho_{c,q}$ at $z/h = 1$ for the imposed (LES) values, as well as the results obtained by each partitioning method. A “cluster” of markers of the same color contains points with the same R/P ratio but different E/T ratios, and the different clusters thus have different R/P (as indicated by arrows of increasing R and E). Both panels contain only flux combinations falling in the range $-P/ET - 0.15 < T/ET < -P/ET + 0.15$, as shown in the delimited region in Figure 5.

722 0, the increase of respiration or evaporation both invariably lead to an increase in W/W_f
 723 given that $W_f = F_c/ET$ decreases when R increases (for a constant P) or when E in-
 724 creases (constant T). However, when $W/W_f < 0$, a further increase in R leads to a de-
 725 crease in the ratio W/W_f , while an increase in E causes its increase (arrows in Figure
 726 13a). The transition in the sign of W/W_f occurs at different values of $\rho_{c,q}$ depending on

727 the height, but clearly the ratio of water-use efficiencies is better defined when canopy
 728 components dominate the total fluxes and $W/W_f > 0$.

729 The relation between T/ET and $\rho_{c,q}$ is shown in Figure 13b. CEC predicts a good
 730 agreement, on average, with the true T/ET ratios, while CEA underestimates the true
 731 ratios (note that CEA outperforms CEC in other regions of the phase diagram that were
 732 not included following the condition $-P/RP - 0.15 < T/ET < -P/RP + 0.15$). The
 733 CECw method clearly diverges from the expected trends for $\rho_{c,q} > 0.50$, performing
 734 similarly to the other methods when plant components become more important ($\rho_{c,q} <$
 735 0). Regarding the FVS method, it underestimates T/ET when $\rho_{c,q}$ is very negative, but
 736 closely follows the expected LES (simulated) values as the correlation coefficient becomes
 737 positive. Overall, the relation between the ratios T/ET and $\rho_{c,q}$ follows the behavior shown
 738 in our previous study (Zahn et al., 2022), which only used field data (although in that
 739 study the true flux components were not known).

740 As previously mentioned, the measurement or parameterization of the water-use
 741 efficiency in field experiments is still a challenge, and its connection to $\rho_{c,q}$ might help
 742 select the best parameterization model, or at least verify their plausibility, under certain
 743 conditions. Therefore, the aim of the previous analysis in this section is to examine whether
 744 we can use $\rho_{c,q}$ as a screening tool for W/W_f , and ecosystem function more broadly. While
 745 such results cannot be generalized or be used for prediction with certainty at this point,
 746 they are a good first step towards obtaining more reliable ecosystem information from
 747 simple eddy-covariance measurements. To this end, we replicated the analyses for water-
 748 use efficiency, as shown in Figure 13, using field data collected at the Treehaven forest
 749 (see section S7 of the SI for a description of the site and data processing). We calculate
 750 W from five different parametrizations of water-use efficiency, and then obtain the ex-
 751 act field-measured W_f and $\rho_{c,q}$. Figure 14 depicts W/W_f versus $\rho_{c,q}$ using these field
 752 data; we show the half-hourly data points, as well as the average ratios (black markers)
 753 in bins of $\Delta\rho_{c,q} = 0.05$.

754 Results for field data show a very similar trend (and magnitudes) to numerical re-
 755 sults, where all models seem to follow a similar increase in the magnitude of W/W_f as
 756 the correlation tends towards zero (from either side). Furthermore, models involving the
 757 water-vapor pressure D (Figures c and d) seem less robust, showing more scatter and/or
 758 lower magnitudes of W/W_f than the remaining models. All models indicate a linear in-
 759 crease of W/W_f with increasingly positive correlation, which might suggest that these
 760 sites experience more variability in respiration than in evaporation (as can be inferred
 761 from the trends shown in figure 13). The same plot over three other NEON sites show
 762 similar results (Section S8 of the SI). Overall, while this analysis cannot evaluate the skill
 763 of a water-use efficiency model, it can increase our confidence in its use given that, on
 764 average, it follows the expected behavior with regards to $\rho_{c,q}$. In addition, filtering out
 765 data points that fall outside the two “clusters” that can be seen in figure 14 for positive
 766 and negative $\rho_{c,q}$ might help exclude periods with higher uncertainties.

767 7 Conclusion

768 We used large-eddy simulations to investigate partitioning methods that are based
 769 on the statistics of turbulent fluctuations of scalar concentrations above canopies. Be-
 770 low we summarize the main findings of this paper.

- 771 1. The intercomparison of turbulent statistics across three different domains — a ho-
 772 mogeneous forest, a “vineyard-like” canopy with parallel rows, and a domain with
 773 square “clusters” of vegetation — revealed how the presence of open gaps of ex-
 774 posed soil impacts partitioning methods. Overall, the larger these canyons (such
 775 as the cluster domain), the greater the turbulent mixing of scalars. As a conse-
 776 quence, mixing of q and c (from soil and canopy) that blurs the soil and vegeta-

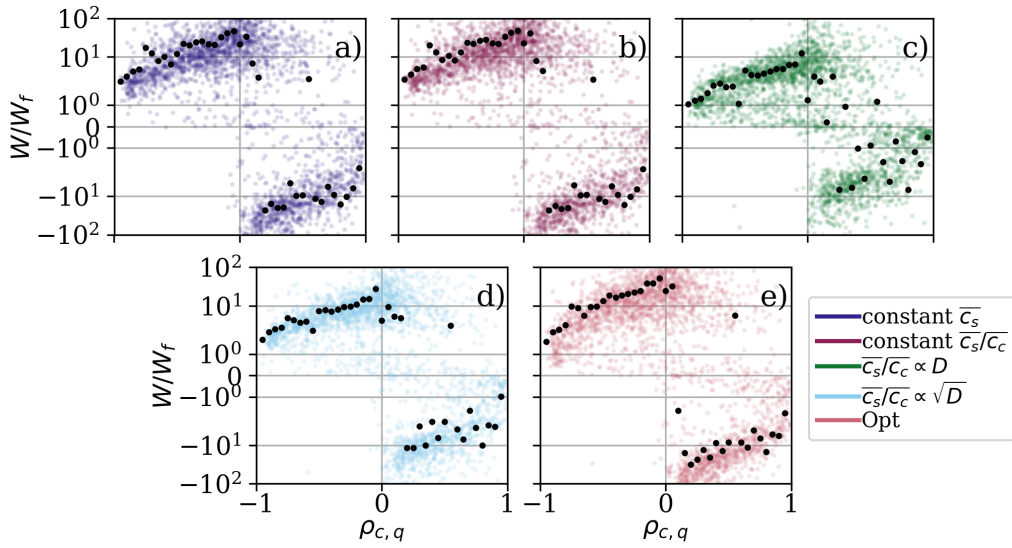


Figure 14. Scatter plot of the ratio W/W_f versus $\rho_{c,q}$ at the NEON site Treehaven (TREE), where $W_f = F_c/ET$. Black markers show the average over intervals $\Delta\rho_{c,q} = 0.05$. Data measured in Spring of 2018 and 2019, only for unstable conditions (*i.e.*, positive heat flux) and when W from all methods were available, are shown. Each plot represents a different parameterization of the water-use efficiency, more specifically the parameterization of the interstomatal CO_2 concentration, \bar{c}_s . These models assume a) constant \bar{c}_s , b) constant ratio between interstomatal and near canopy CO_2 concentration, \bar{c}_s/\bar{c}_c , c) the ratio \bar{c}_s/\bar{c}_c is linearly proportional to vapor-pressure deficit (D), d) the ratio \bar{c}_s/\bar{c}_c is linearly proportional to \sqrt{D} , e) the optimization model proposed by (Scanlon et al., 2019). More details on each model are available in (Zahn et al., 2022).

777 partition signals occurs faster, and at lower heights, when large gaps are present in the
 778 domain. Thus, all partitioning methods were negatively impacted by increased canopy
 779 “openness”. Thus, while vegetation with a low to moderate LAI is still ideal for
 780 partitioning purposes, the presence of wide gaps and large heterogeneity adds more
 781 challenges to the application of these methods.

- 782 2. For CEC, CEA and CECw, the lowest errors in ET partitioning occurred when
 783 the ratios T/E and P/R were proportional. Flux combinations where some meth-
 784 ods performed poorly were usually characterized by atypical combinations, such
 785 as large photosynthesis but negligible transpiration, that are not expected in real
 786 field data. This lends confidence that these methods can provide results with suf-
 787 ficient accuracy to advance the understanding of ecosystems, optimize water-use
 788 in agriculture, or for other practical applications where the carbon-water cycle cou-
 789 pling is important. Nonetheless, more research is needed to determine *a priori* when
 790 (and where) “off-diagonal” conditions are expected.
- 791 3. The best performance of CEC is expected near the canopy top ($z/h \approx 1$) and
 792 when all flux components are non-negligible. CEA yielded comparable results to
 793 CEC, but outperformed the latter at all three levels. CECw also performed well
 794 at the canopy top, and its performance remained almost unaltered at higher lev-
 795 els. For a known water-use efficiency, the FVS method, followed by CECw, are
 796 the most reliable approaches. Therefore, the choice of the best method to apply
 797 hinges on the measurement height, flux ratio, and uncertainty in W .

- 798 4. By combining the CEC method and the water-use efficiency (CECw), we observed
 799 an improvement in the partitioning output relative to the other two methods that
 800 do not use W . Most notably, W helps constraint the magnitude of F_c components,
 801 thus resulting in more accurate flux partitioning for P and R . This underscores
 802 the value of the information that the water-use efficiency adds to simple partition-
 803 ing methods. In addition, given their shared connection through W , we suggest
 804 the concurrent implementation of FVS and CECw as a way to maximize the num-
 805 ber of available solutions over a period.
- 806 5. Partitioning estimates from FVS and CECw respond differently to over and un-
 807 derestimation of the water-use efficiency as well as the flux component combina-
 808 tion themselves. This further motivates the appeal of their co-application since
 809 their weaknesses are not correlated. These results, however, underline the need
 810 for further studies to constrain the range of W over different canopy types and as-
 811 sess its parameterizations.
- 812 6. Conditions when the FVS method yields less valid solutions were identified. Over-
 813 all, high correlation between c and q , in particular $\rho_{c,q} = -1$, explains many of
 814 the conditions when no solutions were found. High correlation tends to occur in
 815 scenarios where *i*) measurements are taken too far from the roughness sublayer,
 816 *ii*) the canopy structures are too open, leading to increased turbulence mixing, and
 817 when *iii*) photosynthesis is much stronger than soil respiration. In addition, less
 818 solutions were also found when W was underestimated from its real value. These
 819 insights can aid in better understanding when and why FVS converges or fails across
 820 different ecosystems.
- 821 7. We identified a connection between the water-use efficiency — a variable inform-
 822 ing us about the plant functioning — and the correlation between q and c , a tur-
 823 bulent quantity. We further showed that this numerical result is in agreement with
 824 field data analyses. This exciting finding opens a path towards recovering biophys-
 825 iological variables from simple high-frequency data measurements.
- 826 8. For readers interested in applying these methods for field data, and given the vari-
 827 ability of the skill and solution availability of the different methods with measure-
 828 ment height, flux ratio, and input uncertainty, our recommendation is to concur-
 829 rently apply all methods, and potentially MREA. This can increase confidence in
 830 the outputs when the methods agree for one or more components, but when they
 831 do not, the various analyses presented here can guide the user on which method
 832 is most likely to be more accurate under given conditions. As an example, figure
 833 S9.1 of the SI intercompares the partitioning components obtained by all meth-
 834 ods above a grass field in Kenya, a dataset previously investigated for partition-
 835 ing by Good et al. (2014) and Zahn et al. (2022). In terms of transpiration, rea-
 836 sonable agreement was found between all methods and the observations obtained
 837 through leaf-level measurements.

838 Because our analyses focused on neutral conditions, we cannot readily extrapolate these
 839 results to all stability conditions. Nonetheless, we hypothesize that as long as no strong
 840 stratification — hindering strong updrafts from carrying soil fluxes — or strong convec-
 841 tion, strongly mixing the scalars — are present, the conclusions we draw in this paper
 842 should still be valid (*i.e.*, for weakly stable or unstable conditions). We also limited our
 843 exploration of canopy domain configuration to three cases; thus, it is possible that dif-
 844 ferent results may emerge if, for instance, the gaps between rows of vegetation were smaller.
 845 Likewise, soil and canopy heterogeneity, including spatial variability of fluxes, LAI and
 846 LAD, are expected in real canopies, but were out of the scope of the present paper. Such
 847 additional analyses are left to future studies.

848 Appendix A Description of Large-eddy simulations

849 The LES algorithm used in this study has been extensively tested over homogeneous
 850 and heterogeneous surfaces, with and without resolved roughness elements (Bou-
 851 Zeid et al., 2005; Kumar et al., 2006; Q. Li & Bou-Zeid, 2019; Huang & Bou-Zeid, 2013;
 852 Zahn & Bou-Zeid, 2023). Its formulation is based on the solution of the spatially filtered
 853 incompressible continuity (equation (A1)) and Navier-Stokes (equation (A2)) equations
 854 under the Boussinesq approximation. The conservation equation for a scalar s (equa-
 855 tion (A3)) is also solved for c_r , c_p , q_e , and q_t . Since only neutral conditions are consid-
 856 ered, the effects of buoyancy are ignored in our analyses. To ensure that our canopy flow
 857 simulations, covering $\approx 14\%$ of the atmospheric boundary layer (ABL ≈ 1 km) height,
 858 closely represent the turbulent profiles expected when the full ABL is simulated, we fol-
 859 lowed the recommendations from Zahn and Bou-Zeid (2023). In this setup, in addition
 860 to a large-scale pressure term, the force balance also includes a stress at the top of the
 861 domain in addition to the Coriolis term. More details are given below and discussed in
 862 Zahn and Bou-Zeid (2023).

$$863 \frac{\partial \tilde{u}_i}{\partial x_i} = 0, \quad (A1)$$

$$864 \frac{\partial \tilde{u}_i}{\partial t} + \tilde{u}_j \left(\frac{\partial \tilde{u}_i}{\partial x_j} - \frac{\partial \tilde{u}_j}{\partial x_i} \right) = - \frac{\partial p^*}{\partial x_i} - \frac{\partial \tau_{ij}}{\partial x_j} + f_c \epsilon_{ij3} (\tilde{u}_j - u_j^G) + D_i, \quad (A2)$$

$$865 \frac{\partial \tilde{s}}{\partial t} + \tilde{u}_j \frac{\partial \tilde{s}}{\partial x_j} = - \frac{\partial \pi_{sj}}{\partial x_j} + S_s. \quad (A3)$$

866 In the above expressions, a filtered variable μ is denoted as $\tilde{\mu}$. \tilde{u}_i is the resolved (filtered)
 867 velocity field ($i=1,2,3$); x_i is the position vector; τ_{ij} is the anisotropic part of the subgrid-
 868 scale (SGS) stress tensor; $f_c = 1.4 \times 10^{-4}$ is the Coriolis parameter; u_j^G is a large scale
 869 pressure forcing imposed in terms of a geostrophic wind; π_{sj} is the SGS scalar flux, and
 870 S_s represents volumetric sinks/sources of the scalar s . A modified resolved dynamic pres-
 871 sure, p^* , is defined to include the resolved and SGS turbulent kinetic energy (Bou-Zeid
 872 et al., 2005). The reference density is taken as 1 and is thus omitted from the equations.
 873 The term D_i represents the drag force exerted by the canopy elements on the flow and
 874 was computed as

$$875 D_i = -C_D a \tilde{u}_i |\tilde{u}_i|, \quad (A4)$$

876 where C_D is the drag coefficient and a is the leaf-area density. The drag coefficient was
 877 modeled following Pan, Follett, et al. (2014),

$$878 C_D = \min \left(\left(\langle \tilde{u}_i \rangle / A \right)^B, C_{D,\max} \right), \quad (A5)$$

879 where A is a velocity scale, B a negative power-law exponent, and $C_{D,\max}$ the maximum
 880 drag coefficient. This formulation represents the change in canopy drag caused by the
 881 variation in the wind speed, which can cause the canopy elements to bend, thus mod-
 882 ifying the canopy resistance through the drag coefficient. As shown by Pan, Follett, et
 883 al. (2014), this drag model improves the representation of higher order statistics. How-
 884 ever, the parameters A , B , and $C_{D,\max}$ are canopy dependent and can be experimen-
 885 tally found if data are available. For our numerical study, we conducted various simu-
 886 lations for different combinations of the parameters tested by Pan, Follett, et al. (2014).
 887 We selected the parameters that resulted in the best comparison between the simula-
 888 tion and the velocity statistics profiles from Su et al. (1998) (more details in the section
 889 3.2). The best match was observed for $A = 0.22$ m/s, $B = -1$, and $C_{D,\max} = 0.3$.

890 The SGS stress is modeled using the scale-dependent Lagrangian dynamic model
 891 (Bou-Zeid et al., 2005), where a constant turbulent SGS Prandtl number of 0.4 is used
 892 to infer the SGS diffusivity and compute the unresolved scalar fluxes. To ensure that the
 893 velocity field satisfies the continuity equation, a Poisson equation is solved for pressure
 894 p^* at every time step. The vertical derivatives are computed by a second-order centered

895 finite difference scheme, implemented on a uniform staggered grid, while a pseudo-spectral
 896 method is implemented for horizontal derivatives. Finally, the explicit second-order Adams-
 897 Bashforth method is used for time stepping.

898 The horizontal boundary conditions are periodic. At the top, we imposed a stress
 899 term, $(\tau_{xz}, \tau_{yz}) = (u_S^2 \cos \alpha, u_S^2 \sin \alpha)$, where u_S is the kinematic stress magnitude and
 900 α is the angle between the stress vector and the x -axis. Following the steps in Zahn and
 901 Bou-Zeid (2023), we used $u_S = 0.3$ m/s and $\alpha = 174^\circ$. In addition, we imposed a stream-
 902 wise large-scale pressure forcing $(u^G, v^G) = (8, 0)$ m/s. Finally, we simulated constant
 903 flux profiles for all scalars by imposing an SGS flux (sink or source) as the top bound-
 904 ary condition for c and q matching the total flux magnitude imposed inside the domain
 905 (ground + canopy).

906 As previously discussed (Su et al., 1998; Watanabe, 2004; Zahn & Bou-Zeid, 2023),
 907 the inclusion of a top stress (and/or scalar flux) results in strong velocity and scalar gra-
 908 dients near the top boundary. However, Watanabe (2004) also showed that their region
 909 of interest ($\approx 70\%$ of the lower domain) was unaffected, resulting in the same turbulence
 910 statistics of a pressure-driven flow. To confirm this finding, we ran individual simulations
 911 driven by a non-zero top stress or by an imposed pressure force, confirming Watanabe
 912 (2004)'s results and also verifying that the partitioning results were consistent and in-
 913 dependent of the choice of the top boundary condition or flow forcing. Nonetheless, we
 914 confine our analyses to the bottom part of the domain, $z \leq 5h$ ($\approx 65\%$ of domain depth).
 915

916

Appendix B Validation of LES setup

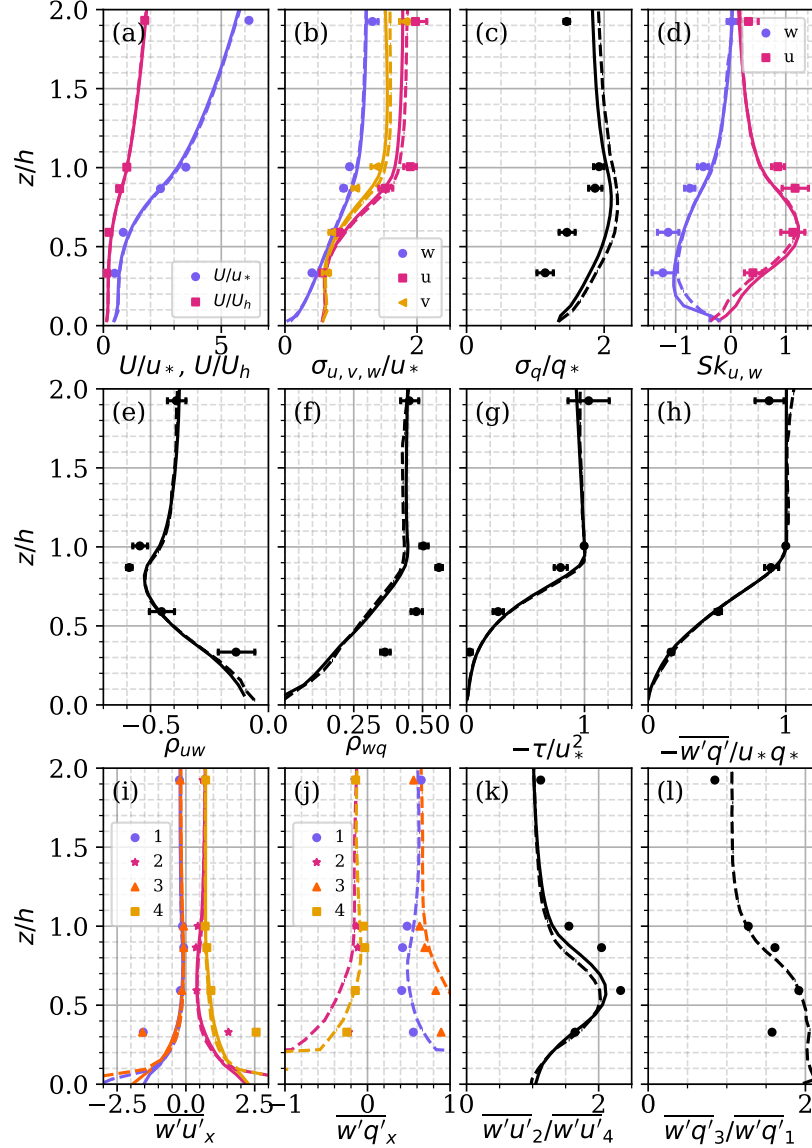


Figure B1. Validation of the LES set-up. Continuous lines represent the spatially and temporally averaged statistics, while dashed lines are the temporal statistics computed from the ensemble average of the 24 virtual eddy-covariance towers, and markers are statistics from a field experiment by (Shaw et al., 1988). Top row shows the velocity profile (a), nondimensional standard deviation of velocity components (b) and water vapor (c), and skewness of u and w (d). The middle row depicts the correlation coefficient between u and w (e) and w and q (f), and the nondimensional stress (g) and water vapor flux profiles (h). The bottom row shows the flux fraction in the four quadrants for momentum (i) and water vapor flux (j), while the ratio between quadrants is shown in (k) (sweeps/ejections) for momentum and (l) for water vapor fluxes.

917 **Open Research Section**

918 The data and models of this paper will be openly shared upon acceptance, and the
 919 details to access them will be provided in this section

920 **Acknowledgments**

921 E.Z. and E.B.Z are supported by the Moore Charitable Foundation Science-to-Action
 922 Fund from the School of Engineering and Applied Science at Princeton, and by the Na-
 923 tional Science Foundation under awards AGS 2128345 and EAR 2126206. We would like
 924 to acknowledge high-performance computing support from Cheyenne (Computational
 925 and Information Systems Laboratory, 2019) and Derecho (Computational and Infor-
 926 mation Systems Laboratory, 2023) provided by NCAR's Computational and Information
 927 Systems Laboratory, sponsored by the National Science Foundation, under projects UPRI0007
 928 and UPRI0021. S.P.G. is supported by the U.S. Department of Energy (Grant DE-SC0024297).
 929 USDA is an equal opportunity provider and employer.

930 **References**

- 931 Allouche, M., Sevostianov, V. I., Zahn, E., Zondlo, M. A., Dias, N. L., Katul, G. G.,
 932 ... Bou-Zeid, E. (2023). Estimating scalar turbulent fluxes with slow-response
 933 sensors in the stable atmospheric boundary layer. *EGUsphere*, 2023, 1–21.
 934 Retrieved from <https://egusphere.copernicus.org/preprints/2023/egusphere-2023-2620/> doi: 10.5194/egusphere-2023-2620
- 935 Baldocchi, D. D. (2003). Assessing the eddy covariance technique for eval-
 936 uating carbon dioxide exchange rates of ecosystems: past, present and fu-
 937 ture. *Global Change Biology*, 9(4), 479–492. Retrieved from <https://onlinelibrary.wiley.com/doi/abs/10.1046/j.1365-2486.2003.00629.x>
 940 doi: <https://doi.org/10.1046/j.1365-2486.2003.00629.x>
- 941 Baldocchi, D. D., Falge, E., Gu, L., Olson, R., Hollinger, D., Running, S., ...
 942 Wofsy, S. (2001). Fluxnet: A new tool to study the temporal and spa-
 943 tial variability of ecosystem-scale carbon dioxide, water vapor, and energy
 944 flux densities. *Bulletin of the American Meteorological Society*, 82(11),
 945 2415 - 2434. Retrieved from https://journals.ametsoc.org/view/journals/bams/82/11/1520-0477_2001_082_2415_fantts_2_3_co_2.xml doi:
 947 10.1175/1520-0477(2001)082(2415:FANTTS)2.3.CO;2
- 948 Baldocchi, D. D., Novick, K., Keenan, T., & Torn, M. (2024). Ameriflux: Its impact
 949 on our understanding of the 'breathing of the biosphere', after 25 years. *Agri-
 950 cultural and Forest Meteorology*, 348. doi: 10.1016/j.agrformet.2024.109929
- 951 Baslam, M., Mitsui, T., Hodges, M., Priesack, E., Herritt, M. T., Aranjuelo, I., &
 952 Sanz-Saez, A. (2020). Photosynthesis in a changing global climate: Scaling
 953 up and scaling down in crops. *Frontiers in Plant Science*, 11. Retrieved from
 954 <https://www.frontiersin.org/articles/10.3389/fpls.2020.00882> doi:
 955 10.3389/fpls.2020.00882
- 956 Bink, N. J., & Meesters, A. G. C. A. (1997).
 957 *Boundary-Layer Meteorology*, 84. doi: 10.1023/A:1000427431944
- 958 Bou-Zeid, E., Meneveau, C., & Parlange, M. (2005). A scale-dependent lagrangian
 959 dynamic model for large eddy simulation of complex turbulent flows. *Physics
 960 of Fluids*, 17(2), 025105. Retrieved from <https://doi.org/10.1063/1.1839152> doi: 10.1063/1.1839152
- 961 Businger, J. A., & Oncley, S. P. (1990). Flux measurement with conditional
 962 sampling. *Journal of Atmospheric and Oceanic Technology*, 7(2), 349–352.
 963 Retrieved from [https://doi.org/10.1175/1520-0426\(1990\)007<0349:FMWCS>2.0.CO;2](https://doi.org/10.1175/1520-0426(1990)007<0349:FMWCS>2.0.CO;2)
- 964 Chen, B., Chamecki, M., & Katul, G. G. (2020). Effects of gentle topography
 965 on forest-atmosphere gas exchanges and implications for eddy-covariance

- 968 measurements. *Journal of Geophysical Research: Atmospheres*, 125(11),
 969 e2020JD032581. Retrieved from <https://agupubs.onlinelibrary.wiley.com/doi/abs/10.1029/2020JD032581> (e2020JD032581
 970 10.1029/2020JD032581) doi: <https://doi.org/10.1029/2020JD032581>
- 971 Computational and Information Systems Laboratory. (2019). *Cheyenne: HPE/SGI
 972 ICE XA System (University Community Computing)*. Boulder, CO: National
 973 Center for Atmospheric Research. doi: 10.5065/D6RX99HX
- 974 Computational and Information Systems Laboratory. (2023). *Derecho: HPE Cray
 975 EX System (University Community Computing)*. Boulder, CO: National Cen-
 976 ter for Atmospheric Research. doi: 10.5065/qx9a-pg09
- 977 Dupont, S., & Brunet, Y. (2008). Influence of foliar density profile on canopy
 978 flow: A large-eddy simulation study. *Agricultural and Forest Meteorol-
 979 ogy*, 148(6), 976-990. Retrieved from <https://www.sciencedirect.com/science/article/pii/S0168192308000336> doi: <https://doi.org/10.1016/j.agrformet.2008.01.014>
- 980 Dusenge, M. E., Duarte, A. G., & Way, D. A. (2019). Plant carbon metabolism
 981 and climate change: elevated co2 and temperature impacts on photosynthesis,
 982 photorespiration and respiration. *New Phytologist*, 221(1), 32-49. Retrieved
 983 from <https://nph.onlinelibrary.wiley.com/doi/abs/10.1111/nph.15283> doi: <https://doi.org/10.1111/nph.15283>
- 984 Edburg, S., Stock, D., Lamb, B., & Patton, E. (2012). The effect of the ver-
 985 tical source distribution on scalar statistics within and above a forest
 986 canopy. *Boundary-Layer Meteorology*, 142(3), 365 – 382. doi: 10.1007/
 987 s10546-011-9686-1
- 988 Eichelmann, E., Mantoani, M. C., Chamberlain, S. D., Hemes, K. S., Oikawa,
 989 P. Y., Szutu, D., ... Baldocchi, D. D. (2022). A novel approach to par-
 990 titioning evapotranspiration into evaporation and transpiration in flooded
 991 ecosystems. *Global Change Biology*, 28(3), 990-1007. Retrieved from
 992 <https://onlinelibrary.wiley.com/doi/abs/10.1111/gcb.15974> doi:
 993 <https://doi.org/10.1111/gcb.15974>
- 994 Fisher, J. B., Tu, K. P., & Baldocchi, D. D. (2008). Global estimates of the
 995 land-atmosphere water flux based on monthly avhrr and islscp-ii data, vali-
 996 dated at 16 fluxnet sites. *Remote Sensing of Environment*, 112(3), 901-919.
 997 Retrieved from <https://www.sciencedirect.com/science/article/pii/S0034425707003938> doi: <https://doi.org/10.1016/j.rse.2007.06.025>
- 998 Good, S. P., Soderberg, K., Guan, K., King, E. G., Scanlon, T. M., & Caylor, K. K.
 999 (2014). $\delta_2\text{H}$ isotopic flux partitioning of evapotranspiration over a grass field
 1000 following a water pulse and subsequent dry down. *Water Resources Research*,
 1001 50(2), 1410-1432. Retrieved from <https://agupubs.onlinelibrary.wiley.com/doi/abs/10.1002/2013WR014333> doi: 10.1002/2013WR014333
- 1002 Hollinger, D. Y., Aber, J., Dail, B., Davidson, E., Goltz, S., Hughes, H., ...
 1003 Walsh, J. (2004). Spatial and temporal variability in forest-atmosphere
 1004 co2 exchange. *Global Change Biology*, 10(10), 1689 – 1706. doi: 10.1111/
 1005 j.1365-2486.2004.00847.x
- 1006 Huang, J., & Bou-Zeid, E. (2013, 6). Turbulence and vertical fluxes in the stable
 1007 atmospheric boundary layer. part i: A large-eddy simulation study. *Journal of
 1008 the Atmospheric Sciences*, 70, 1513-1527. doi: 10.1175/JAS-D-12-0167.1
- 1009 Katul, G. G., Finkelstein, P. L., Clarke, J. F., & Ellestad, T. G. (1996). An inves-
 1010 tigation of the conditional sampling method used to estimate fluxes of active,
 1011 reactive, and passive scalars. *Journal of Applied Meteorology and Climatology*,
 1012 35(10), 1835–1845.
- 1013 Katul, G. G., Goltz, S. M., Hsieh, C.-I., Cheng, Y., Mowry, F., & Sigmon, J. (1995).
 1014 Estimation of surface heat and momentum fluxes using the flux-variance
 1015 method above uniform and non-uniform terrain. *Boundary-Layer Meteo-
 1016 rology*, 74. Retrieved from <https://doi.org/10.1007/BF00712120> doi:
 1017 <https://doi.org/10.1007/BF00712120>

- 1023 10.1007/BF00712120
- 1024 Kirschbaum, M. U. F., & McMillan, A. M. S. (2018). Warming and elevated CO_2
1025 have opposing influences on transpiration. Which is more important? *Current
1026 Forestry Reports*, 4, 51–71. doi: 10.1007/s40725-018-0073-8
- 1027 Klosterhalfen, A., Graf, A., Brüggemann, N., Drüe, C., Esser, O., González-Dugo,
1028 M. P., ... Vereecken, H. (2019). Source partitioning of H_2O and CO_2
1029 fluxes based on high-frequency eddy covariance data: a comparison between
1030 study sites. *Biogeosciences*, 16(6), 1111–1132. Retrieved from <https://www.biogeosciences.net/16/1111/2019/> doi: 10.5194/bg-16-1111-2019
- 1031 Klosterhalfen, A., Moene, A., Schmidt, M., Scanlon, T., Vereecken, H., & Graf, A.
1032 (2019). Sensitivity analysis of a source partitioning method for H_2O and CO_2
1033 fluxes based on high frequency eddy covariance data: Findings from field data
1034 and large eddy simulations. *Agricultural and Forest Meteorology*, 265, 152 -
1035 170. Retrieved from <http://www.sciencedirect.com/science/article/pii/S0168192318303496> doi: <https://doi.org/10.1016/j.agrformet.2018.11.003>
- 1036 Kumar, V., Kleissl, J., Meneveau, C., & Parlange, M. B. (2006). Large-eddy sim-
1037 ulation of a diurnal cycle of the atmospheric boundary layer: Atmospheric
1038 stability and scaling issues. *Water Resources Research*, 42(6). Retrieved
1039 from <https://agupubs.onlinelibrary.wiley.com/doi/abs/10.1029/2005WR004651> doi: <https://doi.org/10.1029/2005WR004651>
- 1040 Lasslop, G., Reichstein, M., Papale, D., Richardson, A. D., Arneth, A., Barr, A., ...
1041 Wohlfahrt, G. (2010). Separation of net ecosystem exchange into assimilation
1042 and respiration using a light response curve approach: critical issues and global
1043 evaluation. *Global Change Biology*, 16(1), 187-208. Retrieved from <https://onlinelibrary.wiley.com/doi/abs/10.1111/j.1365-2486.2009.02041.x>
1044 doi: <https://doi.org/10.1111/j.1365-2486.2009.02041.x>
- 1045 Law, B., Baldocchi, D., & Anthoni, P. (1999). Below-canopy and soil CO_2 fluxes in
1046 a ponderosa pine forest. *Agricultural and Forest Meteorology*, 94(3), 171-188.
1047 Retrieved from <https://www.sciencedirect.com/science/article/pii/S0168192399000192> doi: [https://doi.org/10.1016/S0168-1923\(99\)00019-2](https://doi.org/10.1016/S0168-1923(99)00019-2)
- 1048 Li, Q., & Bou-Zeid, E. (2019). Contrasts between momentum and scalar transport
1049 over very rough surfaces. *Journal of Fluid Mechanics*, 880, 32–58. doi: 10
1050 .1017/jfm.2019.687
- 1051 Li, X., Gentine, P., Lin, C., Zhou, S., Sun, Z., Zheng, Y., ... Zheng, C. (2019). A
1052 simple and objective method to partition evapotranspiration into transpiration
1053 and evaporation at eddy-covariance sites. *Agricultural and Forest Meteo-
1054 rology*, 265, 171 - 182. Retrieved from <http://www.sciencedirect.com/science/article/pii/S016819231830371X> doi: <https://doi.org/10.1016/j.agrformet.2018.11.017>
- 1055 Mao, S., Leclerc, M. Y., & Michaelides, E. E. (2008). Passive scalar flux foot-
1056 print analysis over horizontally inhomogeneous plant canopy using large-
1057 eddy simulation. *Atmospheric Environment*, 42(21), 5446-5458. Re-
1058 tried from <https://www.sciencedirect.com/science/article/pii/S1352231008001908> doi: <https://doi.org/10.1016/j.atmosenv.2008.02.029>
- 1059 Mengis, N., Keller, D. P., Eby, M., & Oschlies, A. (2015, aug). Uncertainty in the
1060 response of transpiration to CO_2 and implications for climate change. *Environ-
1061 mental Research Letters*, 10(9), 094001. Retrieved from <https://dx.doi.org/10.1088/1748-9326/10/9/094001> doi: 10.1088/1748-9326/10/9/094001
- 1062 National Ecological Observatory Network. (2021). *LAI - spectrome-
1063 ter - flightline (dp2.30012.001)*. [https://data.neonscience.org/data-
1065 products/DP2.30012.001/RELEASE-2021](https://data.neonscience.org/data-
1064 products/DP2.30012.001/RELEASE-2021). National Ecological Observatory
1066 Network (NEON). doi: 10.48443/ABRM-BS86
- 1067 National Ecological Observatory Network (NEON). (2022). *Bundled data products
1068 - eddy covariance (dp4.00200.001)*. National Ecological Observatory Network
1069 (NEON). Retrieved from <https://data.neonscience.org/data-products/>
- 1070
- 1071
- 1072
- 1073
- 1074
- 1075
- 1076
- 1077

- 1078 DP4.00200.001/RELEASE-2022 doi: 10.48443/7CQP-3J73
- 1079 Nelson, J. A., Carvalhais, N., Cuntz, M., Delpierre, N., Knauer, J., Ogée, J., ...
 1080 Jung, M. (2018). Coupling water and carbon fluxes to constrain estimates of transpiration: The tea algorithm. *Journal of Geophysical Research: Biogeosciences*, 123(12), 3617-3632. Retrieved from <https://agupubs.onlinelibrary.wiley.com/doi/abs/10.1029/2018JG004727> doi: 10.1029/2018JG004727
- 1085 Nelson, J. A., Pérez-Priego, O., Zhou, S., Poyatos, R., Zhang, Y., Blanken, P. D., ...
 1086 Jung, M. (2020). Ecosystem transpiration and evaporation: Insights from three water flux partitioning methods across fluxnet sites. *Global Change Biology*, n/a(n/a). Retrieved from <https://onlinelibrary.wiley.com/doi/abs/10.1111/gcb.15314> doi: 10.1111/gcb.15314
- 1090 Novick, K., Biederman, J., Desai, A., Litvak, M., Moore, D., Scott, R., & Torn, M. (2018). The ameriflux network: A coalition of the willing. *Agricultural and Forest Meteorology*, 249, 444 – 456. doi: 10.1016/j.agrformet.2017.10.009
- 1093 Pan, Y., Chamecki, M., & Isard, S. A. (2014). Large-eddy simulation of turbulence and particle dispersion inside the canopy roughness sublayer. *Journal of Fluid Mechanics*, 753, 499–534. doi: 10.1017/jfm.2014.379
- 1096 Pan, Y., Follett, E., Chamecki, M., & Nepf, H. (2014). Strong and weak, unsteady reconfiguration and its impact on turbulence structure within plant canopies. *Physics of Fluids*, 26(10), 105102. Retrieved from <https://doi.org/10.1063/1.4898395> doi: 10.1063/1.4898395
- 1100 Pattey, E., Edwards, G., Strachan, I. B., Desjardins, R. L., Kaharabata, S., & Wagner Riddle, C. (2006). Towards standards for measuring greenhouse gas fluxes from agricultural fields using instrumented towers. *Canadian Journal of Soil Science*, 86(3), 373-400. Retrieved from <https://doi.org/10.4141/S05-100> doi: 10.4141/S05-100
- 1105 Paul-Limoges, E., Wolf, S., Eugster, W., Hörtnagl, L., & Buchmann, N. (2017). Below-canopy contributions to ecosystem co2 fluxes in a temperate mixed forest in switzerland. *Agricultural and Forest Meteorology*, 247, 582-596. Retrieved from <https://www.sciencedirect.com/science/article/pii/S0168192317302678> doi: <https://doi.org/10.1016/j.agrformet.2017.08.011>
- 1110 Paul-Limoges, E., Wolf, S., Schneider, F. D., Longo, M., Moorcroft, P., Gharun, M., & Damm, A. (2020). Partitioning evapotranspiration with concurrent eddy covariance measurements in a mixed forest. *Agricultural and Forest Meteorology*, 280, 107786. Retrieved from <https://www.sciencedirect.com/science/article/pii/S0168192319304022> doi: <https://doi.org/10.1016/j.agrformet.2019.107786>
- 1115 Perez-Priego, O., Katul, G. G., Reichstein, M., El-Madany, T. S., Ahrens, B., Carrara, A., ... Migliavacca, M. (2018). Partitioning eddy covariance water flux components using physiological and micrometeorological approaches. *Journal of Geophysical Research: Biogeosciences*, 123(10), 3353-3370. Retrieved from <https://agupubs.onlinelibrary.wiley.com/doi/abs/10.1029/2018JG004637> doi: 10.1029/2018JG004637
- 1120 Reichstein, M., Falge, E., Baldocchi, D., Papale, D., Aubinet, M., Berbigier, P., ... Valentini, R. (2005). On the separation of net ecosystem exchange into assimilation and ecosystem respiration: review and improved algorithm. *Global Change Biology*, 11(9), 1424-1439. Retrieved from <https://onlinelibrary.wiley.com/doi/abs/10.1111/j.1365-2486.2005.001002.x> doi: <https://doi.org/10.1111/j.1365-2486.2005.001002.x>
- 1125 Rigden, A. J., Salvucci, G. D., Entekhabi, D., & Short Gianotti, D. J. (2018). Partitioning evapotranspiration over the continental united states using weather station data. *Geophysical Research Letters*, 45(18), 9605-9613. Retrieved from <https://agupubs.onlinelibrary.wiley.com/doi/abs/10.1029/2018GL079121> doi: <https://doi.org/10.1029/2018GL079121>

- 1133 Rouspard, O., Bonnefond, J.-M., Irvine, M., Berbigier, P., Nouvellon, Y., Dauzat,
 1134 J., ... Bouillet, J.-P. (2006). Partitioning energy and evapo-transpiration
 1135 above and below a tropical palm canopy. *Agricultural and Forest Meteorol-*
 1136 *ogy*, 139(3), 252-268. Retrieved from <https://www.sciencedirect.com/science/article/pii/S0168192306001663> doi: <https://doi.org/10.1016/j.agrformet.2006.07.006>
- 1139 Scanlon, T. M., & Kustas, W. P. (2010). Partitioning carbon dioxide and water
 1140 vapor fluxes using correlation analysis. *Agricultural and Forest Meteorol-*
 1141 *ogy*, 150(1), 89 - 99. Retrieved from <http://www.sciencedirect.com/science/article/pii/S0168192309002214> doi: <https://doi.org/10.1016/j.agrformet.2009.09.005>
- 1144 Scanlon, T. M., & Sahu, P. (2008). On the correlation structure of water vapor
 1145 and carbon dioxide in the atmospheric surface layer: A basis for flux par-
 1146 titioning. *Water Resources Research*, 44(10). Retrieved from <https://agupubs.onlinelibrary.wiley.com/doi/abs/10.1029/2008WR006932> doi:
 1147 [10.1029/2008WR006932](https://doi.org/10.1029/2008WR006932)
- 1149 Scanlon, T. M., Schmidt, D. F., & Skaggs, T. H. (2019). Correlation-based flux
 1150 partitioning of water vapor and carbon dioxide fluxes: Method simplification
 1151 and estimation of canopy water use efficiency. *Agricultural and Forest Me-*
 1152 *teorology*, 279, 107732. Retrieved from <http://www.sciencedirect.com/science/article/pii/S016819231930348X> doi: <https://doi.org/10.1016/j.agrformet.2019.107732>
- 1155 Scott, R. L., & Biederman, J. A. (2017). Partitioning evapotranspiration using long-
 1156 term carbon dioxide and water vapor fluxes. *Geophysical Research Letters*,
 1157 44(13), 6833-6840. Retrieved from <https://agupubs.onlinelibrary.wiley.com/doi/abs/10.1002/2017GL074324> doi: [10.1002/2017GL074324](https://doi.org/10.1002/2017GL074324)
- 1159 Shaw, R. H., Den Hartog, G., & Neumann, H. H. (1988). Influence of foliar
 1160 density and thermal stability on profiles of reynolds stress and turbulence
 1161 intensity in a deciduous forest. *Boundary-Layer Meteorology*, 45. doi:
 1162 [10.1007/BF00124010](https://doi.org/10.1007/BF00124010)
- 1163 Shaw, R. H., & Schumann, U. (1992). Large-eddy simulation of turbulent flow
 1164 above and within a forest. *Boundary-Layer Meteorology*, 61. doi: [10.1007/BF02033994](https://doi.org/10.1007/BF02033994)
- 1166 Skaggs, T., Anderson, R., Alfieri, J., Scanlon, T., & Kustas, W. (2018). Fluxpart:
 1167 Open source software for partitioning carbon dioxide and water vapor fluxes.
 1168 *Agricultural and Forest Meteorology*, 253-254, 218 - 224. Retrieved from
 1169 <http://www.sciencedirect.com/science/article/pii/S0168192318300698> doi: <https://doi.org/10.1016/j.agrformet.2018.02.019>
- 1171 Stoll, R., Gibbs, J. A., Salesky, S. T., Anderson, W., & Calaf, M. (2020, August).
 1172 Large-eddy simulation of the atmospheric boundary layer. *Boundary-Layer
 1173 Meteorology*, 177(2-3), 541-581. Retrieved from <http://dx.doi.org/10.1007/s10546-020-00556-3> doi: [10.1007/s10546-020-00556-3](https://doi.org/10.1007/s10546-020-00556-3)
- 1175 Stoy, P. C., El-Madany, T. S., Fisher, J. B., Gentine, P., Gerken, T., Good, S. P., ...
 1176 Wolf, S. (2019). Reviews and syntheses: Turning the challenges of partitioning
 1177 ecosystem evaporation and transpiration into opportunities. *Biogeosciences*,
 1178 16(19), 3747-3775. Retrieved from <https://www.biogeosciences.net/16/3747/2019/> doi: [10.5194/bg-16-3747-2019](https://doi.org/10.5194/bg-16-3747-2019)
- 1180 Su, H.-B., Shaw, R. H., Paw, K. T., Moeng, C.-H., & Sullivan, P. P. (1998). Turbu-
 1181 lent statistics of neutrally stratified flow within and above a sparse forest from
 1182 large-eddy simulation and field observations. *Boundary-Layer Meteorology*, 88.
 1183 doi: [10.1023/A:1001108411184](https://doi.org/10.1023/A:1001108411184)
- 1184 Sulman, B. N., Roman, D. T., Scanlon, T. M., Wang, L., & Novick, K. A. (2016).
 1185 Comparing methods for partitioning a decade of carbon dioxide and water
 1186 vapor fluxes in a temperate forest. *Agricultural and Forest Meteorology*,
 1187 226-227, 229 - 245. Retrieved from <http://www.sciencedirect.com/>

- 1188 science/article/pii/S0168192316302994 doi: <https://doi.org/10.1016/j.agrformet.2016.06.002>

1189 Thomas, C. K., Martin, J., Goeckede, M., Siqueira, M., Foken, T., Law, B., ...

1190 Katul, G. G. (2008). Estimating daytime subcanopy respiration from conditional sampling methods applied to multi-scalar high frequency turbulence time series. *Agricultural and Forest Meteorology*, 148(8), 1210 - 1229.

1191 Retrieved from <http://www.sciencedirect.com/science/article/pii/S0168192308000737> doi: <https://doi.org/10.1016/j.agrformet.2008.03.002>

1192 Thomas, C. K., Martin, J. G., Law, B. E., & Davis, K. (2013). Toward biologically meaningful net carbon exchange estimates for tall, dense canopies: Multi-level eddy covariance observations and canopy coupling regimes in a mature douglas-fir forest in oregon. *Agricultural and Forest Meteorology*, 173, 14 - 27. Retrieved from <http://www.sciencedirect.com/science/article/pii/S0168192313000051> doi: <https://doi.org/10.1016/j.agrformet.2013.01.001>

1193 Wagle, P., Skaggs, T. H., Gowda, P. H., Northup, B. K., & Neel, J. P. (2020). Flux variance similarity-based partitioning of evapotranspiration over a rainfed alfalfa field using high frequency eddy covariance data. *Agricultural and Forest Meteorology*, 285-286, 107907. Retrieved from <http://www.sciencedirect.com/science/article/pii/S0168192320300095> doi: <https://doi.org/10.1016/j.agrformet.2020.107907>

1194 Wagle, P., Skaggs, T. H., Gowda, P. H., Northup, B. K., Neel, J. P. S., & Anderson, R. G. (2021). Evaluation of water use efficiency algorithms for flux variance similarity-based evapotranspiration partitioning in c3 and c4 grain crops. *Water Resources Research*, 57(5), e2020WR028866. Retrieved from <https://agupubs.onlinelibrary.wiley.com/doi/abs/10.1029/2020WR028866> doi: <https://doi.org/10.1029/2020WR028866>

1195 Wang, K., Bastos, A., Ciais, P., Wang, X., Rodenbeck, C., Gentine, P., ... Piao, S. (2022). Regional and seasonal partitioning of water and temperature controls on global land carbon uptake variability. *Nature Communications*, 13. Retrieved from <https://doi.org/10.1038/s41467-022-31175-w> doi: [10.1038/s41467-022-31175-w](https://doi.org/10.1038/s41467-022-31175-w)

1196 Watanabe, T. (2004). Large-eddy simulation of coherent turbulence structures associated with scalar ramps over plant canopies. *Boundary-Layer Meteorology*, 112, 307-341. doi: <https://doi.org/10.1023/B:BOUN.0000027912.84492.54>

1197 Wei, Z., Yoshimura, K., Wang, L., Miralles, D. G., Jasechko, S., & Lee, X. (2017). Revisiting the contribution of transpiration to global terrestrial evapotranspiration. *Geophysical Research Letters*, 44(6), 2792-2801. Retrieved from <https://agupubs.onlinelibrary.wiley.com/doi/abs/10.1002/2016GL072235> doi: [10.1002/2016GL072235](https://doi.org/10.1002/2016GL072235)

1198 Wilson, K. B., Hanson, P. J., Mulholland, P. J., Baldocchi, D. D., & Wullschleger, S. D. (2001). A comparison of methods for determining forest evapotranspiration and its components: sap-flow, soil water budget, eddy covariance and catchment water balance. *Agricultural and Forest Meteorology*, 106(2), 153-168. Retrieved from <https://www.sciencedirect.com/science/article/pii/S0168192300001994> doi: [https://doi.org/10.1016/S0168-1923\(00\)00199-4](https://doi.org/10.1016/S0168-1923(00)00199-4)

1199 Xu, L., Baldocchi, D. D., & Tang, J. (2004). How soil moisture, rain pulses, and growth alter the response of ecosystem respiration to temperature. *Global Biogeochemical Cycles*, 18(4). Retrieved from <https://agupubs.onlinelibrary.wiley.com/doi/abs/10.1029/2004GB002281> doi: <https://doi.org/10.1029/2004GB002281>

1200 Yue, W., Parlange, M. B., Meneveau, C., Zhu, W., van Hout, R., & Katz, J. (2007). Large-eddy simulation of plant canopy flows using plant-scale representation. *Boundary-Layer Meteorology*, 124. doi: [10.1007/s10546-007-9173-x](https://doi.org/10.1007/s10546-007-9173-x)

- 1242 Zahn, E., & Bou-Zeid, E. (2023). Setting up a large-eddy simulation to fo-
1243 cus on the atmospheric surface layer. *Boundary-Layer Meteorology*. Re-
1244 tried from <https://doi.org/10.1007/s10546-023-00841-x> doi:
1245 10.1007/s10546-023-00841-x
- 1246 Zahn, E., Bou-Zeid, E., & Dias, N. L. (2023). Relaxed eddy accumulation out-
1247 performs monin-obukhov flux models under non-ideal conditions. *Geophys-
1248 ical Research Letters*, 50(7), e2023GL103099. Retrieved from <https://agupubs.onlinelibrary.wiley.com/doi/abs/10.1029/2023GL103099>
1249 (e2023GL103099 2023GL103099) doi: <https://doi.org/10.1029/2023GL103099>
- 1250 Zahn, E., Bou-Zeid, E., Good, S. P., Katul, G. G., Thomas, C. K., Ghannam,
1251 K., ... Kustas, W. P. (2022). Direct partitioning of eddy-covariance wa-
1252 ter and carbon dioxide fluxes into ground and plant components. *Agri-
1253 cultural and Forest Meteorology*, 315, 108790. Retrieved from <https://www.sciencedirect.com/science/article/pii/S0168192321004767> doi:
1254 <https://doi.org/10.1016/j.agrformet.2021.108790>
- 1255 Zhou, S., Yu, B., Zhang, Y., Huang, Y., & Wang, G. (2016). Partitioning evap-
1256 otranspiration based on the concept of underlying water use efficiency.
1257 *Water Resources Research*, 52(2), 1160-1175. Retrieved from <https://agupubs.onlinelibrary.wiley.com/doi/abs/10.1002/2015WR017766> doi:
1258 10.1002/2015WR017766
1259
1260
1261